

Coupling ultracold matter to dynamical gauge fields in optical lattices: From flux attachment to 2 lattice gauge theories

*Original*

Coupling ultracold matter to dynamical gauge fields in optical lattices: From flux attachment to 2 lattice gauge theories / Barbiero, L.; Schweizer, C.; Aidelsburger, M.; Demler, E.; Goldman, N.; Grusdt, F.. - In: SCIENCE ADVANCES. - ISSN 2375-2548. - ELETTRONICO. - 5:10(2019), p. eaav7444. [10.1126/sciadv.aav7444]

*Availability:*

This version is available at: 11583/2959502 since: 2022-03-25T13:43:40Z

*Publisher:*

American Association for the Advancement of Science

*Published*

DOI:10.1126/sciadv.aav7444

*Terms of use:*

This article is made available under terms and conditions as specified in the corresponding bibliographic description in the repository

*Publisher copyright*

(Article begins on next page)

## PHYSICS

# Coupling ultracold matter to dynamical gauge fields in optical lattices: From flux attachment to $\mathbb{Z}_2$ lattice gauge theories

Luca Barbiero<sup>1</sup>, Christian Schweizer<sup>2,3,4</sup>, Monika Aidelsburger<sup>2,3,4</sup>, Eugene Demler<sup>5</sup>, Nathan Goldman<sup>1</sup>, Fabian Grusdt<sup>4,5,6\*</sup>

From the standard model of particle physics to strongly correlated electrons, various physical settings are formulated in terms of matter coupled to gauge fields. Quantum simulations based on ultracold atoms in optical lattices provide a promising avenue to study these complex systems and unravel the underlying many-body physics. Here, we demonstrate how quantized dynamical gauge fields can be created in mixtures of ultracold atoms in optical lattices, using a combination of coherent lattice modulation with strong interactions. Specifically, we propose implementation of  $\mathbb{Z}_2$  lattice gauge theories coupled to matter, reminiscent of theories previously introduced in high-temperature superconductivity. We discuss a range of settings from zero-dimensional toy models to ladders featuring transitions in the gauge sector to extended two-dimensional systems. Mastering lattice gauge theories in optical lattices constitutes a new route toward the realization of strongly correlated systems, with properties dictated by an interplay of dynamical matter and gauge fields.

## INTRODUCTION

Gauge fields play a central role in a wide range of physical settings: The interactions in the standard model are mediated by gauge bosons, and everyday phenomena related to electromagnetism are governed by Maxwell's equations featuring a gauge symmetry. The presence of strong magnetic fields can lead to strong alterations of the behavior of interacting many-body systems; for example, in the fractional quantum Hall (FQH) effect, the statistics of elementary excitations can be transmuted from fermionic to bosonic or to neither of both (anyonic) (1). Last, gauge theories even play a role in strongly correlated quantum systems, where local constraints lead to emergent gauge symmetries at low energies; for example, frustrated quantum spin liquids can be classified by their corresponding gauge theories.

The realization of artificial gauge fields in ultracold gases is an important milestone, enabling studies of the interplay between gauge fields and strong interactions in quantum many-body systems. This feat has further promoted these quantum-engineered systems as versatile quantum simulators (2, 3). While a synthetic magnetic field can be simply introduced by rotating atomic clouds (4, 5), more sophisticated schemes were developed to generate a wide family of gauge field structures, including spin-orbit couplings (6) or patterns featuring staggered magnetic fluxes with alternating signs on a length scale given by the lattice constant (7–9). The design of magnetic fluxes for ultracold atoms in optical lattices, through laser-induced tunneling or shaking methods, has been recently exploited in view of realizing topological states of matter (10, 11) and frustrated magnetism (8). In the settings described above, artificial gauge fields are treated as

classical and nondynamical; however, in the sense that they remain insensitive to the spatial configuration and motion of the atomic cloud, these engineered systems do not aim to reproduce a complete gauge theory, where particles and gauge fields influence each other.

To be able to use ultracold atoms and simulate a wider range of physical problems, including those from high-energy physics, two major steps need to be taken. First, the synthetic gauge fields need to be made intrinsically dynamical, allowing back-actions of the particles on the gauge field. For example, the strength of the synthetic magnetic field may depend explicitly on the local particle density. In a second step, the dynamics of the synthetic gauge fields needs to be constrained to fulfill certain local symmetries. Therefore, the synthetic gauge field interacts with the matter particles, but each lattice site is also associated with a separately conserved charge. Theories of this type are called lattice gauge theories (LGTs), and the detailed conservation laws they satisfy depend on the respective gauge group (12). The simplest instant of an LGT has a  $\mathbb{Z}_2$ , or Ising, gauge group, but in the presence of fermionic matter, even this model poses a substantial theoretical challenge (13).

Various theoretical works have already suggested several methods by which synthetic gauge fields can be made intrinsically dynamical. A first approach builds on the rich interplay between laser-induced tunneling and strong on-site interactions, which can be both present and finely controlled in an optical lattice (3): Under specific conditions, the tunneling matrix elements, which not only describe the hopping on the lattice but also capture the presence of a gauge field, can become density dependent (14–18); see (19) for an experimental implementation of these density-dependent gauge fields. While these settings include rich physics, they lack local conservation laws and thus still differ significantly from problems relevant to, e.g., high-energy physics.

A second approach aims at directly implementing genuine LGTs with local conservation laws, such as the Kogut-Susskind or quantum link models. This can be achieved, in principle, by engineering specific model Hamiltonians through elaborate laser-coupling schemes involving different atomic species and well-designed constraints; see (20–22) for reviews and (23) for an ion trap realization of the Kogut-Susskind

Copyright © 2019  
The Authors, some  
rights reserved;  
exclusive licensee  
American Association  
for the Advancement  
of Science. No claim to  
original U.S. Government  
Works. Distributed  
under a Creative  
Commons Attribution  
NonCommercial  
License 4.0 (CC BY-NC).

<sup>1</sup>Center for Nonlinear Phenomena and Complex Systems, Université Libre de Bruxelles, CP 231, Campus Plaine, B-1050 Brussels, Belgium. <sup>2</sup>Fakultät für Physik, Ludwig-Maximilians-Universität, Schellingstr. 4, 80799 München, Germany. <sup>3</sup>Max-Planck-Institut für Quantenoptik, Hans-Kopfermann-Str. 1, 85748 Garching, Germany. <sup>4</sup>Munich Center for Quantum Science and Technology (MCQST), Schellingstr. 4, D-80799 München Germany. <sup>5</sup>Department of Physics, Harvard University, Cambridge, MA 02138, USA. <sup>6</sup>Department of Physics, Technical University of Munich, 85748, Garching, Germany.

\*Corresponding author. Email: fabian.grusdt@tum.de

Hamiltonian. A digital implementation of  $\mathbb{Z}_2$  LGTs, including couplings to fermionic matter, was proposed in (24). These quantum simulations of LGTs aim to deepen our understanding of fundamental concepts of gauge theories (20–23, 25), such as confinement and its interplay with dynamical charges, which are central in high-energy (26) and condensed-matter physics (13, 27, 28) and go beyond a mere density dependence of synthetic gauge fields. While important first steps have been taken, the direct quantum simulation of LGTs is still in its infancy. The implementations proposed so far still contain significant technical challenges that need to be overcome, making alternative implementation schemes desirable.

In this work, we demonstrate how  $\mathbb{Z}_2$  LGTs can be realized in ultracold gases through the use of specifically designed density-dependent gauge fields. Our approach combines the experimental advantages afforded by settings with density-dependent synthetic gauge fields and the additional physical structure added by the presence of local conservation laws. We demonstrate how existing ultracold atom technology can be used to implement toy models relevant to both high-energy and condensed-matter physics, and describe how the procedure can be scaled up to transition from simplistic two-site models to two-dimensional (2D) systems with direct relevance to studies of, e.g., high-temperature superconductivity (13).

As a central ingredient, we devise a scheme to engineer flux attachment for cold atoms moving in an optical lattice. Originally introduced by Wilczek (29, 30), and then widely exploited in the context of the FQH effect (1), flux attachment is a mathematical construction according to which a certain amount of magnetic flux quanta is attached to a particle (e.g., an electron). The resulting composite “flux tube particle” can change its quantum statistics from bosonic to fermionic, or vice versa (30), and naturally appears in field theoretical formulations of FQH states (1). Specifically, we show that an optical lattice loaded with two atomic species ( $a$  and  $f$ ) can be configured in a way that a localized  $f$ -particle becomes a source of magnetic flux  $\Phi$  for the  $a$ -particle: The magnetic flux can thus effectively be attached to the  $f$ -particles, which are also allowed to move around the lattice (see Fig. 1A). (Cases with only one species, more closely related to the FQH effect, can also be considered.) The flux attachment scheme is our starting point for implementing  $\mathbb{Z}_2$  LGTs using ultracold atoms.

For specific choices of parameters and carefully designed lattice geometries, we first show that this appealing setting can be readily used to implement interacting quantum systems with  $\mathbb{Z}_2$  link variables and global  $\mathbb{Z}_2$  gauge symmetries. Then, we demonstrate that our method can also be extended to systems with local symmetries, realizing genuine  $\mathbb{Z}_2$  LGTs (26) in various lattice geometries. These latter types of models, where the matter field couples to a  $\mathbb{Z}_2$  lattice gauge field, are especially relevant in the context of high- $T_c$  superconductivity (13, 31) and, more generally, strongly correlated electrons (32–34). A central question in this context concerns the possibility of a confinement-deconfinement transition in the LGT (12), which would indicate electron fractionalization (13, 35, 36). The proposed model will allow us to explore the interplay of a global  $U(1)$  symmetry with local  $\mathbb{Z}_2$  symmetries, which has attracted particular attention in the context of high- $T_c$  cuprate compounds (34, 37, 38).

We discuss in detail the physics of a toy model characterized by a global  $U(1) \times \mathbb{Z}_2$  symmetry, which consists of a two-leg ladder geometry and can be directly accessed with state-of-the-art cold atom experiments. We demonstrate that the toy model features an intricate interplay of matter and gauge fields, as a result of which the system

undergoes a phase transition in the  $\mathbb{Z}_2$  sector depending on the ratio of the species-dependent tunnel couplings  $t^a/t^f$  (see Fig. 1B). While this transition can be characterized by the spontaneously broken global  $\mathbb{Z}_2$  symmetry, we argue that an interpretation in terms of the constituents of a  $\mathbb{Z}_2$  LGT (see Fig. 1C) is nevertheless useful to understand its microscopic origin. We also predict a phase transition of the matter field from an insulating Mott state to a gapless superfluid (SF) regime, associated with the spontaneously broken global  $U(1)$  symmetry. For appropriate model parameters, an interplay of both types of transitions can be observed.

The paper is organized as follows. We start by introducing the flux attachment scheme, which is at the heart of the proposed experimental implementation of dynamical gauge fields. Particular attention is devoted to the case of a double-well system, which forms the common building block for realizing  $\mathbb{Z}_2$  LGTs coupled to matter. Next, we study the phase diagram of a toy model with a two-leg ladder geometry, consisting of a matter field coupled to a  $\mathbb{Z}_2$  gauge field on the rungs. Realistic

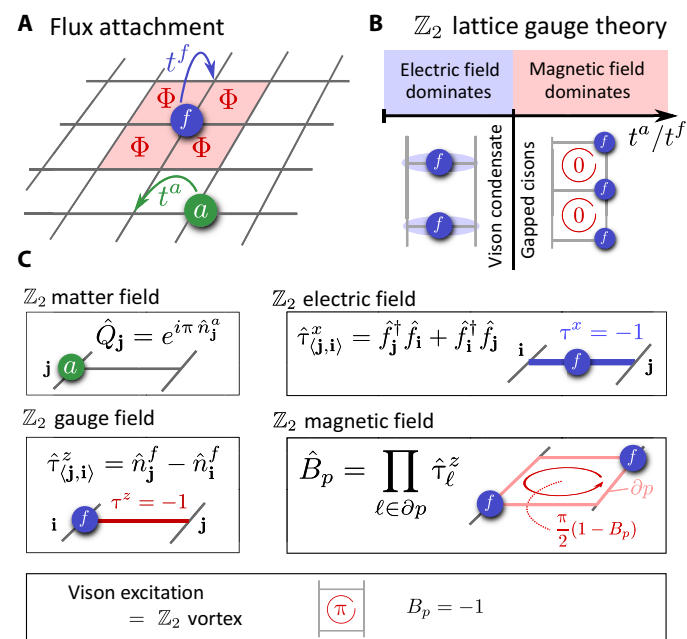


**Fig. 1. Flux-attachment and dynamical gauge fields with ultracold atoms.** (A) We propose a setup where one atomic species  $f$  becomes a source of magnetic flux  $\Phi$  (red) for a second species  $a$ . Both types of atoms undergo coherent quantum dynamics, described by NN tunneling matrix elements  $t^a$  and  $t^f$ , respectively. (B) When realized in a ladder geometry, the flux attachment setup has a  $\mathbb{Z}_2$  lattice gauge structure. By tuning the ratio of the tunneling elements  $t^a/t^f$ , we find that the system undergoes a phase transition. The two regimes can be understood in terms of the elementary ingredients of a  $\mathbb{Z}_2$  LGT, summarized in (C). The matter field  $\hat{a}$  has a  $\mathbb{Z}_2$  charge given by the parity of its occupation numbers  $\hat{n}^a$ . It couples to the  $\mathbb{Z}_2$  gauge field  $\hat{\tau}_{(j,i)}^z$ , defined as the number imbalance of the  $f$ -particles between different ends of a link. When  $|t^a| \ll |t^f|$ , the ground state is dominated by tunneling of the  $f$ -particles, realizing that eigenstates of the  $\mathbb{Z}_2$  electric field  $\hat{\tau}_{(j,i)}^x$  delocalized over the link. In the opposite limit,  $|t^a| \gg |t^f|$ , the tunneling dynamics of the  $a$ -particles prevails and the system realizes eigenstates of the  $\mathbb{Z}_2$  magnetic field  $\hat{B}_p$ , defined as a product of the gauge field  $\hat{\tau}_\ell^z$  over all links  $\ell \in \partial p$  along the edge of a plaquette  $p$ . The  $\mathbb{Z}_2$  magnetic field introduces Aharonov-Bohm phases for the matter field, which are  $0$  ( $\pi$ ) when the  $f$  particles occupy the same (different) leg of the ladder, i.e., if  $B_p = 1$  ( $B_p = -1$ ). The quantized excitations of the dynamical gauge field correspond to  $\mathbb{Z}_2$  vortices of the Ising gauge field, so-called visons.

implementations of the considered models are proposed afterward, along with a scheme for realizing genuine  $\mathbb{Z}_2$  LGTs with local instead of global symmetries in two dimensions. This paves the way for future investigations of strongly correlated systems, as discussed in the summary and outlook section.

The minimal model of a  $\mathbb{Z}_2$  LGT coupled to matter proposed here has been realized experimentally in a double-well system (39). Besides, density-dependent Peierls phases have been realized with two-component fermions in (40), based on a two-frequency driving scheme, which is proposed below as an ingredient to implement  $\mathbb{Z}_2$  LGTs in extended lattices.

## RESULTS

### Flux attachment

The recent experimental implementations of classical gauge fields for ultracold atoms (41–45) combine two key ingredients (46): First, the bare tunnel couplings  $t$  are suppressed by large energy offsets  $|\Delta| \gg t$ , realized by a magnetic field gradient or a superlattice potential. Second, tunneling is restored with complex phases  $\phi$  by proper time modulation of the optical lattice (47, 48) at the resonance frequency  $\omega = \Delta$  (with  $\hbar = 1$  throughout). The phase of the lattice shaking directly determines the value  $\phi$  of the complex hopping element.

Flux attachment operates in a strongly correlated regime, where the energy offsets  $\Delta = \omega$  from an external potential are supplemented by interspecies Hubbard interactions of the same magnitude,  $U = \omega$  (49). This provides coherent control over the synthetic gauge fields induced by the lattice modulation at frequency  $\omega$  [see also (14–18)].

We consider a situation where atoms of a first species, with annihilation operators  $\hat{a}$ , represent a matter field. The atoms of the second type, associated with annihilation operators  $\hat{f}$ , will become the sources of synthetic magnetic flux for the matter field (see Fig. 1A). Namely, the magnetic flux felt by the  $a$ -particle, as captured by its assisted hopping over the lattice, is only effective in the presence of an  $f$ -particle. To avoid that—vice versa—the  $f$ -particles become subject to magnetic flux created by the  $a$ -particles, static potential gradients affecting only the  $f$ -particles are used. In the following, we assume that both atomic species are hard-core bosons, although generalizations are possible, for instance, when one or both of them are replaced by fermions.

### Model

The largest energy scale in our problem is set by strong interspecies Hubbard interactions

$$\hat{\mathcal{H}}_{\text{int}} = U \sum_j \hat{n}_j^a \hat{n}_j^f \quad (1)$$

where  $\hat{n}_j^{a,f}$  denote the density operators of  $a$ - and  $f$ -particles on lattice site  $j$ . To break the symmetry between  $a$ - and  $f$ -particles, we introduce state-dependent static potentials  $V_\alpha(j)$ , where  $\alpha = a, f$ . We assume that the corresponding energy offsets between nearest-neighbor (NN) lattice sites  $i$  and  $j$  are integer multiples  $m_{(i,j)}^\alpha \in \mathbb{Z}$  of the large energy scale  $U$ , up to small corrections  $|\delta V_{(i,j)}^\alpha| \ll U$ , which are acceptable, namely

$$\Delta_{(i,j)}^\alpha \equiv V_\alpha(i) - V_\alpha(j) \approx m_{(i,j)}^\alpha U \quad (2)$$

A minimal example is illustrated in Fig. 2A.

Coherent dynamics of both fields are introduced by NN tunneling matrix elements in the  $\mu = x, y$  directions,  $t_\mu^\alpha$ , respectively. Thus, the free part of the Hamiltonian is

$$\hat{\mathcal{H}}_0 = - \sum_{\mu=x,y} \sum_{\langle i,j \rangle_\mu} \left[ t_\mu^a \hat{a}_i^\dagger \hat{a}_j + t_\mu^f \hat{f}_j^\dagger \hat{f}_i + \text{h.c.} \right] + \sum_j \left[ V_a(j) \hat{n}_j^a + V_f(j) \hat{n}_j^f \right] \quad (3)$$

where  $\langle i, j \rangle_\mu$  denotes a pair of NN sites along direction  $\mu$ . Tunnel couplings are initially suppressed by the external potentials  $\Delta^\alpha = m^\alpha U$  and the strong Hubbard interactions

$$U \gg |t_{x,y}^\alpha| \quad (4)$$

To restore tunnel couplings with complex phases, we include a time-dependent lattice modulation

$$\hat{\mathcal{H}}_\omega(t) = \sum_j V_\omega(j, t) (\hat{a}_j^\dagger \hat{a}_j + \hat{f}_j^\dagger \hat{f}_j) \quad (5)$$

It acts equally on both species and is periodic in time,  $V_\omega(j, t + 2\pi/\omega) = V_\omega(j, t)$ , with frequency  $\omega = U$  resonant with the interspecies interactions. In summary, our Hamiltonian is

$$\hat{\mathcal{H}}(t) = \hat{\mathcal{H}}_0 + \hat{\mathcal{H}}_{\text{int}} + \hat{\mathcal{H}}_\omega(t) \quad (6)$$

### Effective hopping Hamiltonian

From now on, we consider resonant driving,  $U = \omega \gg |t_{x,y}^\alpha|$ , where the lattice modulation  $\hat{\mathcal{H}}_\omega(t)$  in Eq. 5 restores, or renormalizes, all

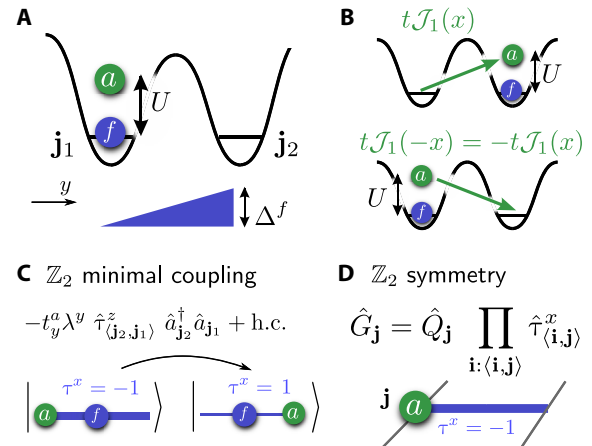


**Fig. 2.  $\mathbb{Z}_2$  LGT in a two-well system.** (A) We consider a double-well setup with one atom of each type,  $a$  and  $f$ . Coherent tunneling between the two orbitals at  $j_1$  and  $j_2 = j_1 + \mathbf{e}_y$  is suppressed for both species by strong Hubbard interactions  $U = \omega$ , and for  $f$ -particles by the energy offset  $\Delta^f = \omega$  indicated by the blue triangle. (B) Tunnel couplings can be restored by resonant lattice modulations with frequency  $\omega$ . The sign of the restored tunneling matrix element is different when the  $a$ -particle gains (top) or loses (bottom) energy. (C) This difference in sign gives rise to the  $\mathbb{Z}_2$  gauge structure and allows the implementation of  $\mathbb{Z}_2$  minimal coupling of the matter field  $\hat{a}$  to the link variable defined by the  $f$ -particles. The action of this term in the effective Hamiltonian acting on a basis state (left) is illustrated. The strength of the  $\mathbb{Z}_2$  electric field is indicated by the thickness of the blue line connecting the two sites of the double-well system. The minimal coupling term is the common building block for realizing larger systems with a  $\mathbb{Z}_2$  gauge structure. (D) These systems are characterized by a symmetry  $\hat{G}_j$  associated with each lattice site  $j$ . Here,  $\hat{G}_j$  commutes with the Hamiltonian and consists of the product of the  $\mathbb{Z}_2$  charge,  $\hat{Q}_j = (-1)^{\hat{n}_j^f}$ , and all electric field lines—for which  $\tau^x = -1$ —emanating from a volume around site  $j$ .

tunnel couplings of  $a$ - and  $f$ -particles. As derived in Materials and Methods, we obtain an effective hopping Hamiltonian to lowest order in  $1/\omega$

$$\hat{\mathcal{H}}_{\text{eff}} = - \sum_{\mu=x,y} \sum_{\langle i,j \rangle_{\mu}} \left[ t_{\mu}^a \hat{a}_i^{\dagger} \hat{a}_j \hat{\lambda}_{(i,j)\mu}^{\mu} e^{i\hat{\phi}_{(i,j)\mu}^{\mu}} + \text{h.c.} \right. \\ \left. + t_{\mu}^f \hat{f}_i^{\dagger} \hat{f}_j \hat{\Lambda}_{(i,j)\mu}^{\mu} e^{i\hat{\theta}_{(i,j)\mu}^{\mu}} + \text{h.c.} \right] \quad (7)$$

The Hermitian operators  $\hat{\lambda}_{(i,j)\mu}^{\mu}$  and  $\hat{\phi}_{(i,j)\mu}^{\mu}$  ( $\hat{\Lambda}_{(i,j)\mu}^{\mu}$  and  $\hat{\theta}_{(i,j)\mu}^{\mu}$ , respectively) in Eq. 7 describe the renormalization of the tunneling amplitudes and phases for  $a$  (respectively  $f$ ) particles; they are mutually commuting and depend only on the number imbalance  $\hat{n}_j^a - \hat{n}_i^a$  (respectively  $\hat{n}_j^f - \hat{n}_i^f$ ) associated with the respective complementary species. Our result in Eq. 7 is reminiscent of the models discussed in (17).

Explicit expressions for  $\hat{\lambda}$ ,  $\hat{\phi}$ ,  $\hat{\Lambda}$ , and  $\hat{\theta}$  can be obtained by considering their matrix elements on the relevant many-body states  $|\psi_r\rangle$  and  $|\psi_s\rangle$  in the Fock basis that are involved in the various hopping processes. For an  $a$ -particle transitioning from state  $|\psi_s\rangle$  to  $|\psi_r\rangle$ , corresponding to a relative potential and/or interaction energy offset  $\Delta_{rs} = n_{rs}\omega$  with integer  $n_{rs} \in \mathbb{Z}$ , the matrix elements are given by

$$\langle \psi_r | \hat{a}_i^{\dagger} \hat{a}_j \hat{\lambda}_{(i,j)\mu}^{\mu} | \psi_s \rangle = | \mathcal{J}_{n_{rs}}(x) | \quad (8)$$

Here  $\mathcal{J}_n$  denotes the Bessel function of the first kind,  $x = A_{ij}/\omega$  is the dimensionless driving strength, and

$$V_{\omega}(\mathbf{i}, t) - V_{\omega}(\mathbf{j}, t) = A_{ij} \cos(\omega t + \phi_{i,j}) \quad (9)$$

Without loss of generality, we assume  $\omega, A_{ij} > 0$  throughout the paper.

The complex phases of the restored tunnelings are also determined by the many-body energy offsets  $\Delta_{rs} = n_{rs}\omega$ . If  $n_{rs} \geq 0$ , the particle gains energy in the hopping process and

$$\langle \psi_r | \hat{a}_i^{\dagger} \hat{a}_j \hat{\phi}_{(i,j)\mu}^{\mu} | \psi_s \rangle = | n_{rs} | \phi_{i,j} \quad (10)$$

In contrast, if  $n_{rs} < 0$ , the particle loses energy and

$$\langle \psi_r | \hat{a}_i^{\dagger} \hat{a}_j \hat{\phi}_{(i,j)\mu}^{\mu} | \psi_s \rangle = | n_{rs} | (\pi - \phi_{i,j}) \quad (11)$$

In this case, there is an additional  $n_{rs}\pi$  phase shift due to the reflection properties of the Bessel function,  $J_n(-x) = (-1)^n J_n(x)$  (see Fig. 2B). This  $n_{rs}\pi$  phase shift is at the core of the LGT implementations discussed below. Similar results are obtained for  $\hat{\Lambda}_{(i,j)\mu}^{\mu}$  and  $\hat{\theta}_{(i,j)\mu}^{\mu}$  by exchanging the roles of  $a$  and  $f$  (see the ‘‘Two-particle two-site problem’’ section in Materials and Methods). Note, however, that the symmetry between  $a$  and  $f$  can be broken by a careful design of the potentials  $V_a$  and  $V_f$ , and this will be exploited in the next paragraph.

As illustrated in Fig. 1A, our scheme allows us to implement effective Hamiltonians (Eq. 7) describing a mixture of two species, where one acts as a source of magnetic flux for the other [see also (17)]. A detailed discussion of the resulting Harper-Hofstadter model with dynamical gauge flux is provided in section S1. By analogy with the physics of the FQH effect (50, 51), we expect that this flux attachment

gives rise to interesting correlations and possibly to quasiparticle excitations with nontrivial statistics.

### $\mathbb{Z}_2$ LGT in a double well

Now, we apply the result in Eq. 7 and discuss a minimal setting, where one  $a$ -particle and one  $f$ -particle each tunnel between the two sites  $\mathbf{j}_1$  and  $\mathbf{j}_2 = \mathbf{j}_1 + \mathbf{e}_y$  of a double-well potential (see Fig. 2A);  $\mathbf{e}_y$  denotes the unit vector along  $y$ . This system forms the central building block for the implementation of  $\mathbb{Z}_2$  LGTs in larger systems, proposed below. We assume that  $V_a(\mathbf{j}_i) \equiv 0$  for  $i = 1, 2$  but introduce a potential offset  $V_f(\mathbf{j}_2) = \Delta^f + V_f(\mathbf{j}_1)$  for the  $f$  species, breaking the symmetry between  $a$ - and  $f$ -particles.

*Effective Hamiltonian.* For  $\Delta^f = U = \omega$  and lattice modulations with a trivial phase  $\phi_{j_1, j_2} = 0$ , the effective Floquet Hamiltonian in Eq. 7 becomes

$$\hat{\mathcal{H}}_{\text{eff}}^{2\text{well}} = -t_y^a \lambda^y \hat{\tau}_{(j_2, j_1)}^z (\hat{a}_{j_2}^{\dagger} \hat{a}_{j_1} + \text{h.c.}) - t_y^f \hat{\Lambda} \hat{\tau}_{(j_2, j_1)}^x \quad (12)$$

with notations defined as follows. We describe the  $f$ -particle by a pseudo-spin- $\frac{1}{2}$

$$\hat{\tau}_{(j_2, j_1)}^z = \hat{n}_{j_2}^f - \hat{n}_{j_1}^f, \quad \hat{n}_{j_2}^f + \hat{n}_{j_1}^f = 1 \quad (13)$$

which becomes a link variable in a  $\mathbb{Z}_2$  LGT (see Fig. 1C). The Pauli matrix  $\hat{\tau}_{(j_2, j_1)}^x = (\hat{f}_{j_2}^{\dagger} \hat{f}_{j_1} + \text{h.c.})$  describes tunneling of the  $f$ -particle.

As shown in Fig. 2B, the interaction energy of the matter field changes by  $\pm U$  in every tunneling event. As a result, the amplitude renormalization in Eq. 12 is  $\lambda^y = | \mathcal{J}_1(A_{j_2, j_1}/\omega) |$  (see Eq. 8), and the phase of the restored tunnel couplings is  $e^{i\hat{\phi}} = \hat{\tau}_{(j_2, j_1)}^z$  by Eqs. 10 and 11. Because the  $f$ -particle is subject to an additional potential offset  $\Delta^f = U$  between the two sites, its energy can only change by 0 or  $2U$  in a tunneling event. Hence, the phase of the restored tunneling in Eq. 12 is trivial,  $\hat{\theta} = 0$  as in Eqs. 10 and 11, but the amplitude renormalization

$$\hat{\Lambda} = \mathcal{J}_0(A_{j_2, j_1}/\omega) \hat{n}_{j_1}^a + \mathcal{J}_2(A_{j_2, j_1}/\omega) \hat{n}_{j_2}^a \quad (14)$$

depends on the configuration of the  $a$ -particle in general.

The effective Hamiltonian (Eq. 12) realizes a minimal version of a  $\mathbb{Z}_2$  LGT: The link variable  $\hat{\tau}_{(j_2, j_1)}^z \simeq e^{i\pi \hat{A}}$  provides a representation of the dynamical  $\mathbb{Z}_2$  gauge field  $\hat{A}$ , which is quantized to 0 and 1. The corresponding  $\mathbb{Z}_2$  electric field is given by the Pauli matrix  $\hat{\tau}_{(j_2, j_1)}^x$ , defining electric field lines on the link. The  $\mathbb{Z}_2$  charges  $\hat{Q}_i$ , defined on the two sites  $\mathbf{j}_i$  with  $i = 1, 2$ , are carried by the  $a$ -particle,  $\hat{Q}_i = \exp(i\pi \hat{n}_i^a)$ . These ingredients are summarized in Fig. 1C and justify our earlier notion that the  $a$ - and  $f$ -particles describe matter and gauge fields, respectively. The Hamiltonian in Eq. 12 realizes a minimal coupling (12) of the  $a$ -particles to the gauge field (see Fig. 2C).

*Symmetries.* Each of the two lattice sites  $\mathbf{j}_i$  is associated with a  $\mathbb{Z}_2$  symmetry. The operators generating the  $\mathbb{Z}_2$  gauge group in the double-well system

$$\hat{g}_i = \hat{Q}_i \hat{\tau}_{(j_2, j_1)}^x, \quad \mathbf{i} = 1, 2 \quad (15)$$

both commute with the effective Hamiltonian in Eq. 12,  $[\hat{g}_i, \hat{\mathcal{H}}_{\text{eff}}^{2\text{well}}] = 0$  for  $i = 1, 2$ . This statement is not entirely trivial for the first term in Eq. 12: While  $\hat{\tau}_{(j_2, j_1)}^z$  and  $\hat{a}_{j_2}^{\dagger} \hat{a}_{j_1}$  do not commute with  $\hat{\tau}_{(j_2, j_1)}^x$  and  $\hat{Q}_i$

individually, their product commutes with  $\hat{g}_f$ . The second term in Eq. 12 trivially commutes with  $\hat{g}_i$  because  $[\hat{\Lambda}, \hat{Q}_i] = 0$  (see Eq. 14).

Physically, Eq. 15 establishes a relation between the  $\mathbb{Z}_2$  electric field lines,  $\tau_{\langle j_2, j_1 \rangle}^x = -1$ , and the  $\mathbb{Z}_2$  charges from which they emanate (see Fig. 2D). Note that the eigenvalues of  $\hat{g}_1$  and  $\hat{g}_2$  are not independent, because  $\hat{g}_1 \hat{g}_2 = -1$  for the considered case with a single  $a$ -particle tunneling in the double-well system.

The model in Eq. 12 is invariant under the gauge symmetries  $\hat{g}_i$  for all values of the modulation strength  $A_{j_2, j_1}$ . In general, both terms in the effective Hamiltonian couple the  $\mathbb{Z}_2$  charge to the gauge field. An exception is obtained for lattice modulation strengths  $A_{j_2, j_1}/\omega = x_{02}$  for which

$$\mathcal{J}_0(x_{02}) = \mathcal{J}_2(x_{02}) \quad (16)$$

In this case, neither of the amplitude renormalizations

$$\hat{\Lambda} \rightarrow \Lambda_{02} = \mathcal{J}_0(x_{02}) \approx 0.32 \quad (17)$$

$$\lambda^y = \lambda_{02} = \mathcal{J}_1(x_{02}) \approx 0.58 \quad (18)$$

is operator valued, and the second term in the Hamiltonian only involves the  $\mathbb{Z}_2$  gauge field. The weakest driving for which Eq. 16 is satisfied has  $x_{02} \approx 1.84$ .

*Intuition.* We take this opportunity to explain in a mechanistic way the meaning of the  $\mathbb{Z}_2$  gauge field in the double-well system and its relation to more general LGTs. As a starting point, consider the situation when  $t_y^f = 0$  and the  $f$ -particle is localized. Depending on the position of the  $f$  atom (left or right), the restored tunneling amplitude of the  $a$ -atom between the two sites has a sign  $\pm 1$ . Formally, this corresponds to the appearance of the factor  $\hat{\tau}_{\langle j_2, j_1 \rangle}^z = \hat{n}_{j_2}^f - \hat{n}_{j_1}^f$  in the first term on the left hand side of Eq. 12. At this point, we have realized a synthetic gauge field  $\mathcal{A}_{\langle j_2, j_1 \rangle}$  for the  $a$ -atoms, which depends on the density of the  $f$ -atoms. That is, the general tunneling matrix element of the  $a$ -particles,  $\hat{t}_{j_2, j_1}^a e^{i\pi \mathcal{A}_{\langle j_2, j_1 \rangle}}$ , has a phase  $\pi \mathcal{A}_{\langle j_2, j_1 \rangle}$  depending on the  $f$ -density.

The two possible states of the link variable, corresponding to the two positions  $j_1$  and  $j_2$  of the  $f$  atom, define a 2D Hilbert space on the link  $\langle j_2, j_1 \rangle$ . This Hilbert space is equivalent to the Hilbert space of a  $\mathbb{Z}_2$  lattice gauge field, with two orthogonal states on each link of the lattice. Using this language, we can identify the operator  $\hat{\tau}_{\langle j_2, j_1 \rangle}^z$  with a  $\mathbb{Z}_2$  gauge field. It does not commute with the corresponding  $\mathbb{Z}_2$  electric field operator,  $\hat{\tau}_{\langle j_2, j_1 \rangle}^x$ , which corresponds physically to the coherence of the  $f$ -atom between the two sites  $j_2$  and  $j_1$ . This non-commutativity is related to the noncommutativity of the conjugate electric and magnetic fields  $\hat{e}$  and  $\hat{B}$  in quantum electrodynamics. Because of the small  $\mathbb{Z}_2$  gauge group, the  $\mathbb{Z}_2$  electric field only takes two possible quantized values:  $\hat{\tau}_{\langle j_2, j_1 \rangle}^x = \pm 1$ . The eigenstates correspond to even and odd superpositions of the  $f$ -atom on the two lattice sites:  $(\hat{f}_{j_2}^\dagger \pm \hat{f}_{j_1}^\dagger) |0\rangle / \sqrt{2}$ .

If we allow to add arbitrary perturbations to the tunneling Hamiltonian, e.g., terms  $\delta_y \hat{\tau}_{\langle j_2, j_1 \rangle}^y$  or  $\delta_z \hat{\tau}_{\langle j_2, j_1 \rangle}^z$ , we can introduce non-trivial dynamics of the synthetic gauge field. While this renders the density-dependent synthetic gauge field dynamical, it does not correspond to a  $\mathbb{Z}_2$  LGT in the strict sense, since local conservation laws are generically absent. These situations, without local conservation laws, lead to interesting physics nonetheless and have been studied for example in the context of the so-called  $\mathbb{Z}_2$  Bose-Hubbard model (52, 53).

A genuine  $\mathbb{Z}_2$  LGT is obtained if only terms are included in the Hamiltonian, which commute with the  $\mathbb{Z}_2$  gauge operators  $\hat{g}_i$  in Eq. 15. In particular, this includes the term  $t_y^f \hat{\Lambda} \hat{\tau}_{\langle j_2, j_1 \rangle}^x$  on the right hand side of Eq. 12 or simpler terms such as  $t_y^f \hat{\tau}_{\langle j_2, j_1 \rangle}^x$ . These are the  $\mathbb{Z}_2$  analogs of terms  $\sim E^2$  in the Hamiltonian of quantum electrodynamics, without the square due to the simpler nature of the  $\mathbb{Z}_2$  gauge group. In the double-well system, the  $\mathbb{Z}_2$  gauge symmetry leads to two decoupled sectors of the Hamiltonian with  $g_1 = -g_2 = 1$  and  $g_1 = -g_2 = -1$ . As will be shown later, however, in extended systems, each lattice site is associated with its own conserved charge. This has important consequences for the possible many-body phases (12).

### Matter gauge field coupling in two-leg ladders

In the following, we study the physics of coupled matter and gauge fields in a two-leg ladder, accessible with numerical density matrix renormalization group (DMRG) simulations (54). Our starting point is a model with minimal couplings to the  $\mathbb{Z}_2$  gauge field on the rungs of the ladder, which is characterized by a global  $U(1) \times \mathbb{Z}_2$  symmetry (see Fig. 3A). Here, we study its phase diagram. As explained later, the model can be implemented relatively easily in existing ultracold atom setups by coupling multiple double-well systems, which is our main motivation for studying its phase diagram.

#### The model

We combine multiple double-well systems (Eq. 12) to a two-leg ladder by introducing tunnelings  $t_x^a$  of the matter field along  $x$ . Furthermore, we impose that the  $f$ -particles can only move along the rungs,  $t_x^f = 0$ , and each rung is occupied by one  $f$ -particle. Thus, we can continue describing the  $f$  degrees of freedom by link variables  $\hat{\tau}_{\langle i, j \rangle}$ , as defined in Eq. 13. The number of  $a$ -particles  $N_a$  will be freely tunable.

*Effective Hamiltonian.* For a properly designed configuration of lattice gradients and modulations, presented in detail later, we obtain an effective Hamiltonian

$$\begin{aligned} \hat{\mathcal{H}}_{2\text{leg}} = & - \sum_{\langle i, j \rangle_x} \left( t_x^a \hat{\Lambda}_{\langle i, j \rangle_x}^x \hat{a}_j^\dagger \hat{a}_i + \text{h.c.} \right) \\ & - \sum_{\langle i, j \rangle_y} \left[ t_y^a \lambda^y \left( \hat{a}_j^\dagger \hat{a}_i \hat{\tau}_{\langle i, j \rangle}^z + \text{h.c.} \right) \right. \\ & \left. + t_y^f \hat{\Lambda}_{\langle i, j \rangle}^y \hat{\tau}_{\langle i, j \rangle}^x \right] \end{aligned} \quad (19)$$

Expressions for the amplitude renormalizations  $\lambda^y \in \mathbb{R}$  and  $\hat{\Lambda}^x, \hat{\Lambda}^y$  are provided in section S2B.

For the specific set of driving strengths  $x = x_{02}$  that we encountered already in the double-well problem (see Eq. 16), we find that  $\hat{\Lambda}^y$  only has a weak dependence on the  $\mathbb{Z}_2$  charges,  $\hat{Q}_j = (-1)^{\hat{n}_j^a}$ . Similarly, the amplitude renormalization  $\lambda^x$  depends weakly on the  $\mathbb{Z}_2$  magnetic field  $\hat{B}_p$  only; here

$$\hat{B}_p = \prod_{\langle i, j \rangle \in \partial p} \hat{\tau}_{\langle i, j \rangle}^z \quad (20)$$

is defined as a product over all links  $\langle i, j \rangle$  on the rungs belonging to the edge  $\partial p$  of plaquette  $p$ . Hence, for these specific modulation strengths

$$[\hat{\Lambda}_{\langle i, j \rangle}^y, \hat{Q}_l] = [\hat{\Lambda}_{\langle i, j \rangle}^y, \hat{\tau}_{\langle k, l \rangle}] = 0 \quad (21)$$

$$[\hat{\Lambda}_{\langle i, j \rangle_x}^x, \hat{Q}_p] = [\hat{\Lambda}_{\langle i, j \rangle_x}^x, \hat{a}_l^{(\dagger)}] = 0 \quad (22)$$

**Symmetries.** Now, we discuss the symmetries of the effective Hamiltonian (Eq. 19) at the specific value of the driving strengths  $x_{02}$ . In the case of decoupled rungs, i.e., for  $t_x^a = 0$ , every double well commutes with  $\hat{g}_i$ ,  $i = 1, 2$  from Eq. 15. These symmetries are no longer conserved for  $t_x^a \neq 0$ ; in this general case, a global  $Z_2$  gauge symmetry remains

$$\hat{V}_i = \prod_{j=1}^{L_x} \hat{g}_i(je_x), \quad i = 1, 2 \quad (23)$$

with  $\hat{g}_i(je_x) = (-1)^{\hat{Q}_{jex+(i-1)ey}} \hat{\tau}_{(jex+ey, jex)}^x$  and for which  $\hat{V}_i^2 = 1$ . Using Eqs. 21 and 22, one readily confirms that  $[\hat{\mathcal{H}}_{2\text{leg}}, \hat{V}_i] = 0$  for  $i = 1, 2$ .

In summary, the effective model is characterized by the global  $U(1)$  symmetry associated with the conservation of the number of  $a$ -particles and the global  $Z_2$  symmetry  $\hat{V}_1$ . Note that the second  $Z_2$  symmetry,  $\hat{V}_2$ , follows as a consequence of combining  $\hat{V}_1$  with the global  $U(1)$  symmetry: By performing the global  $U(1)$  gauge transformation  $\hat{a}_j \rightarrow -\hat{a}_j$  for all sites  $j$ ,  $\hat{V}_2$  is obtained from  $\hat{V}_1$ . Thus, the overall symmetry is  $U(1) \times Z_2$ .

**Physical constituents.** In the following, we will describe the physics of the ladder models using the ingredients of  $Z_2$  LGTs (see Fig. 1C). The quantized excitations of the  $Z_2$  lattice gauge field are vortices of the  $Z_2$  (or Ising) lattice gauge field, so-called visons (13). They are defined on the plaquettes of the ladder: If the plaquette term in Eq. 20 is  $B_p = 1$ , there is no vison on  $p$ ; the presence of an additional  $Z_2$  flux,  $B_p = -1$ , corresponds to a vison excitation on plaquette  $p$ . Since the matter field  $\hat{a}$  couples to the  $Z_2$  gauge field, the resulting interactions with the visons determine the phase diagram of the many-body Hamiltonian.

### Quantum phase transitions of matter and gauge fields

We start from the microscopic model in Eq. 19 and simplify it by making a mean field approximation for the renormalized tunneling amplitudes, which depend only weakly on  $\hat{Q}_j$  and  $\hat{B}_p$ . Replacing them

by  $C$ -numbers,  $\tilde{t}_x^a = t_x^a \langle \hat{\lambda}^x \rangle$ ,  $\tilde{t}_y^f = t_y^f \langle \hat{\Lambda}^y \rangle$ , and  $\tilde{t}_y^a = t_y^a \lambda^y$  leads to the conceptually simpler Hamiltonian

$$\begin{aligned} \hat{\mathcal{H}}_{2\text{leg}}^{\text{simp}} = & - \sum_{(i,j)_x} \tilde{t}_x^a \left( \hat{a}_j^\dagger \hat{a}_i + \text{h.c.} \right) \\ & - \sum_{(i,j)_y} \left[ \tilde{t}_y^a \left( \hat{a}_j^\dagger \hat{a}_i \hat{\tau}_{(i,j)_y}^z + \text{h.c.} \right) + \tilde{t}_y^f \hat{\tau}_{(i,j)_y}^x \right] \end{aligned} \quad (24)$$

illustrated in Fig. 3A. Later, by introducing a more sophisticated driving scheme, we will show that this model can also be directly implemented using ultracold atoms. The simpler Hamiltonian (Eq. 24) has identical symmetry properties as Eq. 19. Now, we analyze Eq. 24 by means of the DMRG technique. In the phase diagram, we find at least three distinct phases, resulting from transitions in the gauge and matter field sectors (see Fig. 3B). Here, we describe their main features; for more details, the reader is referred to section S4.

**Transition in the matter sector.** First, we concentrate on the conceptually simpler phase transition taking place in the charge sector. When the tunneling along the legs is weak,  $\tilde{t}_x^a \leq [(\tilde{t}_y^f)^2 + (\tilde{t}_y^a)^2]^{1/2} - \tilde{t}_y^a$ , and the number  $N_a$  of  $a$ -particles is tuned, we observe a pronounced rung-Mott phase (55) at the commensurate filling  $N_a = L_x$ , where  $L_x$  denotes the total number of rungs in the system. Similar to the analysis in (56–58), this phase can be characterized by the parity operator

$$O_p(l) = \left\langle \exp \left[ i\pi \sum_{j<l} \left( \hat{n}_{je_x}^a + \hat{n}_{je_x+ey}^a - \frac{N_a}{L_x} \right) \right] \right\rangle \quad (25)$$

In the limit  $l \approx L_x$  and  $L_x \rightarrow \infty$ , the observable  $O_p(l)$  remains finite only in the Mott insulating regime. Our results in Fig. 4A confirm that  $O_p$  takes large values with a weak size dependence for  $N_a = L_x$ . On the other hand, when  $N_a/L_x \neq 1$  is slightly increased or decreased, the parity  $O_p$  immediately becomes significantly smaller and a more

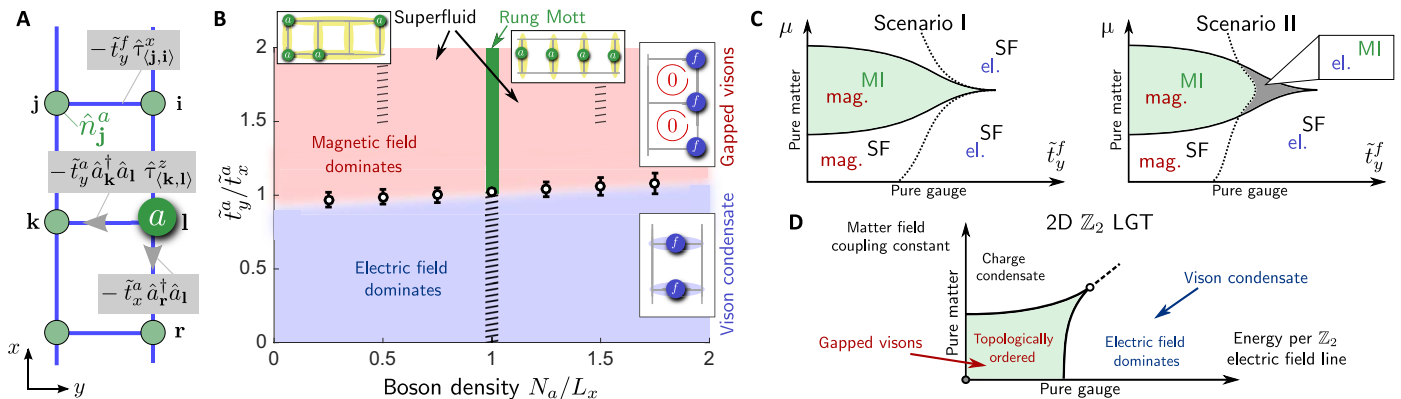


**Fig. 3. Coupling matter to a  $Z_2$  gauge field in a two-leg ladder.** (A) We consider the Hamiltonian (Eq. 24) describing  $a$ -particles that are minimally coupled to the  $Z_2$  gauge field  $\hat{\tau}_{(i,j)_y}^z$  on the rungs of a two-leg ladder. (B) The phase diagram, obtained by DMRG simulations at  $\tilde{t}_y^f/\tilde{t}_x^a = 0.54$ , contains an SF-to-Mott transition in the charge sector at a commensurate density of the matter field,  $N_a = L_x$ . In addition, we find a transition in the gauge sector, from an ordered region with a broken global  $Z_2$  symmetry where the  $Z_2$  magnetic field dominates and the vison excitations of the gauge field are gapped (red) to a disordered regime where the  $Z_2$  electric field is dominant and visons are strongly fluctuating in a condensed state (blue). Along the hatched lines at commensurate fillings  $N_a/L_x = 1/2, 1, 3/2$ , insulating CDW states could exist, but conclusive numerical results are difficult to obtain. (C) The conjectured schematic phase diagram of Eq. 24 is shown in the  $\mu - \tilde{t}_y^f$  plane, where  $\mu$  denotes the chemical potential for  $\hat{a}$  particles and  $2\tilde{t}_y^f$  corresponds to the energy cost per  $Z_2$  electric field line along a rung. Two scenarios are realized in different parameter regimes: In scenario I, the interplay of gauge and matter fields prevents a fully disordered Mott phase, whereas the latter exists in scenario II. The behavior in scenario I resembles the phase diagram of the more general 2D  $Z_2$  LGT (13, 26–28) sketched in (D). In our DMRG simulations here, as well as in the following figures, we keep up to 1400 DMRG states with five finite-size sweeps; the relative error on the energies is kept smaller than  $10^{-7}$ .

pronounced  $L_x$  dependence is observed, consistent with a vanishing value in thermodynamic limit as expected for an SF phase.

For larger values of  $\tilde{t}_x^a$  and  $N_a = L_x$ , no clear signatures of a rung-Mott phase are found (see section S4B): The parity operator  $O_p$  takes significantly smaller values, the calculated Mott gap becomes a small fraction of  $\tilde{t}_x^a$ , consistent with a finite-size gap, and we checked that the decay of two-point correlations follows a power-law at long distances until edge effects begin to play a role. These signatures are consistent with an SF phase.

Because of the global  $U(1)$  symmetry of the model, an SF-to-Mott transition at  $N_a = L_x$  in the quasi-1D ladder geometry would be of Berezinskii-Kosterlitz-Thouless (BKT) type (59). Hence, the gap is strongly suppressed and the correlation length is exponentially large close to the transition point, making it impossible to determine conclusively from our numerical results whether the ground state is a gapped Mott state in this regime. For hard-core bosons on a two-leg ladder, this scenario is realized: It has been shown by bosonization that an infinitesimal interleg coupling is sufficient to open up an exponentially small Mott gap (55, 60).

Similar considerations apply at the commensurate fillings  $N_a/L_x = 1/2, 3/2$ , where previous work on single-component bosons in a two-leg ladder (60) pointed out the possible emergence of an insulating charge density wave (CDW) for large enough  $\tilde{t}_y^a/\tilde{t}_x^a$  (hatched areas in Fig. 3B). Our numerical results indicate that these CDWs may exist in this regime also in our model (Eq. 24). But since the numerical analysis is plagued by a potentially even larger correlation length and a corresponding strongly suppressed Mott gap, it is difficult to pinpoint the exact location of this BKT transition.

The SF phase observed at incommensurate filling fractions is characterized by a power-law decay of the Green's function  $\langle \hat{a}_{de_x}^\dagger \hat{a}_0 \rangle \simeq d^{-1/4K}$  in the charge sector. The exponent is related to the Luttinger parameter  $K$ , which approaches  $K \rightarrow 1/2$  at a transition to the rung-Mott phase for commensurate filling. We confirm this behavior and obtain qualitatively identical results as in the case of a static gauge field (see section S4A for details) (55).

**Transition in the gauge sector.** In the gauge sector, described by  $f$ -particles, we observe a phase transition when the ratios of the tunnel couplings are tuned. In Fig. 4B, we tune  $\tilde{t}_y^a/\tilde{t}_x^a$  while keeping  $\tilde{t}_y^f/\tilde{t}_x^a$  fixed. We find a transition from a symmetric regime where  $\langle \hat{v}_{(i,j)}^z \rangle = 0$  to a region with a nonvanishing order parameter  $\langle \hat{v}_{(i,j)}^z \rangle \neq 0$ . Similar behavior is obtained when tuning  $\tilde{t}_y^f/\tilde{t}_x^a$  while keeping  $\tilde{t}_x^a/\tilde{t}_y^a$  fixed (see section S4E).

The observed transition is associated with a spontaneous breaking of the global  $\mathbb{Z}_2$  symmetry (Eq. 23) of the model. The  $f$ -particles go from a regime where they are equally distributed between the legs,  $\langle \hat{v}_{(i,j)}^z \rangle = 0$ , to a twofold degenerate state with population imbalance,  $\langle \hat{v}_{(i,j)}^z \rangle \neq 0$ . This behavior occurs in the insulating and SF regimes of the charge sector, and it is only weakly affected by the filling value  $N_a/L_x$  (see Fig. 3B).

The two phases are easily understood in the limiting cases. When  $\tilde{t}_y^a = 0$ , the ground state is an eigenstate of the  $\mathbb{Z}_2$  electric field  $\hat{v}_{(i,j)}^z$ , on the rungs, with eigenvalues 1. The  $\mathbb{Z}_2$  magnetic field is strongly fluctuating, and no  $\mathbb{Z}_2$  electric flux loops exist. Thus, also the vison number is strongly fluctuating, and the state can be understood as a vison condensate. In the opposite limit, when  $\tilde{t}_y^a \rightarrow \infty$ , the kinetic energy of the matter field dominates. In this case, the  $\mathbb{Z}_2$  magnetic field is effectively static, and its configuration is chosen to minimize the kinetic energy of the  $a$ -particles. This is achieved when the effective Aharonov-Bohm phases on the plaquettes vanish, i.e., for  $\hat{B}_p = 1$  (see Fig. 1C). In this case, vison excitations with  $\hat{B}_p = -1$  (see Fig. 4C) correspond to localized defects in the system, which cost a finite energy corresponding to the vison gap.

LGTs are characterized by Wilson loops (12). Their closest analogs in our two-leg ladder model are string operators of visons

$$W(d) = \left\langle \prod_{j=1}^d \hat{B}_{p_j} \right\rangle = \langle \hat{v}_{(i,j)}^z \hat{v}_{(i+de_x, j+de_x)}^z \rangle \quad (26)$$

see Fig. 4D. In the disordered phase (electric field dominates), we found numerically that  $W(d) \rightarrow 0$  when  $d \rightarrow \infty$ . Sufficiently far from

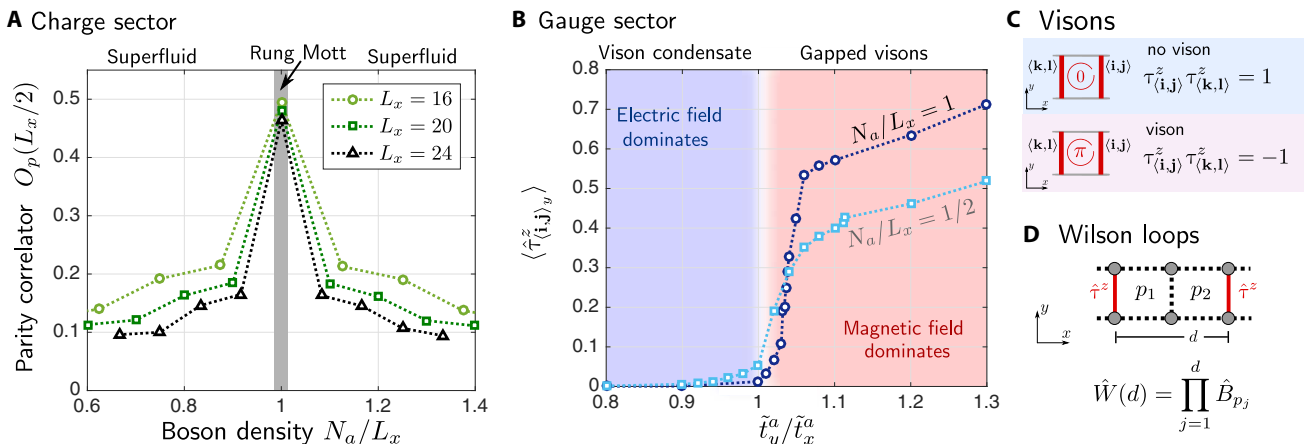


**Fig. 4. Characterizing phase transitions of matter coupled to a  $\mathbb{Z}_2$  gauge field in a two-leg ladder.** We consider the Hamiltonian from Eq. 24. (A) In the charge sector, we observe transitions from an SF state, characterized by a vanishing parity correlator  $O_p(L_x/2 \rightarrow \infty) \rightarrow 0$  in the thermodynamic limit, to an insulating rung-Mott state at the commensurate filling  $N_a = L_x$ , characterized by  $O_p(L_x/2 \rightarrow \infty) > 0$  and exponentially decaying correlations. Here, we present exemplary results for  $\tilde{t}_y^f/\tilde{t}_x^a = 3$  and  $\tilde{t}_y^f/\tilde{t}_x^a = 0.54$ . (B) In the gauge sector, we find a transition from a disordered phase, where the  $\mathbb{Z}_2$  electric field dominates, to a phase where the  $\mathbb{Z}_2$  magnetic field dominates. In the second case, the order parameter  $\langle \hat{v}_{(i,j)}^z \rangle \neq 0$  corresponds to a spontaneously broken global  $\mathbb{Z}_2$  symmetry (23). In the two phases, the corresponding vison excitations of the  $\mathbb{Z}_2$  gauge field (C) have different characteristics. The numerical results in (A) [respectively (B)] are obtained by considering periodic boundary conditions (respectively  $L_x = 96$  rungs with open boundaries). (D) Analogs of Wilson loops  $\hat{W}(d)$  in the two-leg ladder are string operators of visons.



the transition, where finite-size effects are small, our data (see fig. S5) show the expected exponential decay. In the ordered phase (magnetic field dominates),  $W(d) \rightarrow W_\infty$  quickly converges to the nonzero value  $W_\infty = \langle \tilde{v}_{(i,j)}^z \rangle^2 > 0$  when  $d \rightarrow \infty$ . See section S3 (D and E) for more details.

The qualitatively different behavior of the Wilson loop in the two phases is reminiscent of the phenomenology known from the ubiquitous confinement-deconfinement transitions found in  $(2+1)$  dimensional LGTs (12, 13, 26): There, vortices are gapped in the deconfined phase and the Wilson loop decays only weakly exponentially with a perimeter law; in the confining phase, vortices condense and the Wilson loop decays much faster with an exponential area law.

Our numerical results in Fig. 4B indicate that the phase transition in the gauge sector is continuous. Beyond this fact, its nature is difficult to determine. The interactions between the  $\mathbb{Z}_2$  link variables are mediated by the matter field, which has correlations extending over many sites following either a power-law (in the SF regime) or featuring exponential decay with a correlation length  $\xi \gg 1$  (in the considered Mott-insulating regions). On the one hand, this leads to relatively large finite-size effects in our numerical simulations, which explains the continuous onset of the transition in Fig. 4B. On the other hand, when nonlocal Ising interactions mediated by the gapless matter field compete with the transverse  $\mathbb{Z}_2$  electric field term  $\propto \tilde{t}_y^f \tilde{v}_{(i,j)}^x$  in the Hamiltonian, a rich set of critical exponents can be expected (61). For more details, see section S4E.

*Interplay of matter and gauge fields.* Last, we discuss the interplay of the observed phase transitions in the gauge and matter sectors. To this end, we find it convenient to consider the phase diagram in the  $\mu - \tilde{t}_y^f$  plane, where  $\mu$  denotes a chemical potential for the  $a$ -particles and  $\tilde{t}_y^f$  controls fluctuations of the  $\mathbb{Z}_2$  electric field. We collect our result in the schematic plots in Fig. 3C: Deep in the SF phase, realized for small  $\mu$  and  $N_a/L_x < 1$ ,  $\tilde{t}_y^f$  drives the transition in the gauge sector. Because of a particle-hole symmetry of the hard-core bosons in the model, similar results apply for large  $\mu$  and  $N_a/L_x > 1$ . On the other hand, when  $\tilde{t}_y^f$  is small, permitting a sizable Mott gap at commensurate fillings,  $\mu$  drives the SF-to-Mott transition.

More interesting physics can happen at the tip of the Mott lobe for commensurate fillings  $N_a = L_x$ . This corresponds to the hatched regime in Fig. 3B, where we cannot say conclusively if the system is in a gapped Mott phase. To obtain better understanding of the commensurate regime, we first argue that an SF cannot coexist with the ordered phase of the gauge field at commensurate fillings: In this regime, the  $\mathbb{Z}_2$  gauge field acquires a finite expectation value,  $\langle \tilde{v}_{(i,j)}^z \rangle \neq 0$ . This leads to a term in the Hamiltonian  $\sim -\tilde{t}_y^f a \langle \tilde{v}_{(i,j)}^z \rangle \hat{a}_i^\dagger \hat{a}_j$ , which is expected to open a finite Mott gap, following the arguments in (55, 60). Therefore, only the two scenarios shown in Fig. 3C are possible: In the first case, the Mott insulator coexists only with the ordered phase of the gauge field; in the second scenario, the Mott state coexists with the disordered phase of the gauge field.

To shed more light on this problem, we consider the case when the Mott gap  $\Delta$  is much larger than the tunneling  $\tilde{t}_x^a$ . When  $\tilde{t}_x^a = 0$ , every rung represents an effective localized spin-1/2 degree of freedom. As shown in section S4C, finite tunnelings  $\tilde{t}_x^a \ll \Delta$  introduce antiferromagnetic couplings between these localized moments, and in this limit, our system can be mapped to an XXZ chain. It has an Ising anisotropy, and the ground state has a spontaneously broken  $\mathbb{Z}_2$  symmetry everywhere, except when  $\tilde{t}_y^f / \tilde{t}_x^a \rightarrow \infty$ , where an isotropic Heisenberg model is obtained and the ground state has power-law correlations. The transition from the gapped Mott state, correspond-

ing to the ordered phase of the  $\mathbb{Z}_2$  gauge field, to a symmetric state of two decoupled SFs with a disordered gauge field is of BKT type (62).

Our last argument demonstrates that scenario I in Fig. 3C is realized deep in the Mott phase. In this limit of small  $\tilde{t}_x^a$  and strong couplings  $\tilde{t}_y^f$  of the gauge field, our analysis proves that an intricate interplay of the phase transitions in the gauge and matter sectors exists. This behavior, characteristic for scenario I in Fig. 3C, is reminiscent of the phase diagram of the 2D  $\mathbb{Z}_2$  LGT (see Fig. 3D) (26, 28). In that case, the phase at weak couplings has topological order as in Kitaev's toric code (28), and the disordered phases are continuously connected to each other at strong couplings.

On the other hand, a detailed analysis of the Luttinger-K parameter for larger values of  $\tilde{t}_x^a$  shows that the ground state at commensurate filling  $N_a = L_x$  is characterized by  $K = 1/2$ , in both the  $\mathbb{Z}_2$  symmetric and  $\mathbb{Z}_2$  broken regimes (see section S4, A and B). This behavior is indicative of scenario II in Fig. 3C, since the BKT transition is characterized by a value  $K = 1$  of the Luttinger parameter (62).

### Implementation: Coupled double-well systems

Now, we describe how the models discussed above, and extensions thereof, can be implemented in state-of-art ultracold atom setups. The double-well system introduced around Eq. 12 constitutes the building block for implementing larger systems with a  $\mathbb{Z}_2$  gauge symmetry, or even genuine  $\mathbb{Z}_2$  LGTs, because it realizes a minimal coupling of the matter field to the gauge field (see Fig. 2C) (12). We start by discussing the two-leg ladder Hamiltonian  $\hat{\mathcal{H}}_{2\text{leg}}$  (Eq. 19); then, we present a scheme, based on flux attachment, for implementing a genuine  $\mathbb{Z}_2$  LGT coupled to matter in a 2D square lattice.

#### Two-leg ladder geometry

The ladder system shown in Fig. 3A can be obtained by combining multiple double wells (Eq. 12) and introducing tunnelings  $t_x^a$  of the matter field along  $x$ , while  $t_x^f = 0$ . The lattice potential is modulated along  $y$  with amplitude  $A_{j_2, j_1} = V_\omega^y$ , as in the case of a single double well. As described in Fig. 5, we introduce an additional static potential gradient with strength  $\Delta_x^a = U = \omega$  per lattice site along  $x$  and modulate it with frequency  $\omega$  and amplitude  $V_\omega^x$ .

As shown in section S2, this setup leads to the effective Hamiltonian (Eq. 19). For the specific set of driving strengths  $V_\omega^x / \omega = V_\omega^y / \omega = x_{02}$  (see Eq. 16), the amplitude renormalizations are  $\lambda^y = \lambda_{02}$  and

$$\hat{\lambda}_{(i,j)_x}^x = \frac{1}{2} \left( 1 - \tilde{v}_{(\pm e_y, i)}^z \tilde{v}_{(j \pm e_y, j)}^z \right) \mathcal{J}_0(x_{02}) + \frac{1}{2} \left( 1 + \tilde{v}_{(\pm e_y, i)}^z \tilde{v}_{(j \pm e_y, j)}^z \right) \mathcal{J}_1(x_{02}) \quad (27)$$

*Simplified model.* Now, we discuss a further simplification of the model in Eq. 19, leaving its symmetry group unchanged. We note that, even for the specific choice of the driving strengths  $V_\omega^x / \omega = V_\omega^y / \omega = x_{02}$ , the renormalized tunnel couplings of the  $a$ -particles along  $x$  still depend explicitly on the  $\mathbb{Z}_2$  gauge fields on the adjacent rungs (see Eq. 27). This complication can be avoided, by simultaneously modulating the gradient along  $x$  at two frequencies,  $\omega$  and  $2\omega$ , with amplitudes  $V_\omega^x$  and  $V_{2\omega}^x$ ; i.e., we consider the following driving term in Eq. 5

$$V_\omega(j, t) = [j_x V_\omega^x + j_y V_\omega^y] \cos(\omega t) + j_x V_{2\omega}^x \cos(2\omega t) \quad (28)$$

Following (48), we obtain expressions for the restored tunnel couplings along  $x$  for an energy offset  $n\omega$  introduced by the Hubbard interactions  $U = \omega$  between  $a$ - and  $f$ -particles;  $\lambda_n = \sum_{\ell=-\infty}^{\infty} \mathcal{J}_{n-2\ell}(x^{(1)})$

$\mathcal{J}_\ell(x^{(2)}/2)$ , where  $x^{(1)} = V_\omega^x/\omega$  and  $x^{(2)} = V_{2\omega}^x/\omega$  (see section S2). By imposing the conditions  $\lambda_0 = \lambda_1 = \lambda_2$ , we obtain a simplified effective Hamiltonian where  $\hat{\lambda}_{(i,j)x}^x \rightarrow \lambda^x \in \mathbb{R}$  is no longer operator valued, and thus completely independent of the  $\mathbb{Z}_2$  gauge field  $\hat{\tau}^z$ . The weakest driving strengths for which this condition is met are given by

$$x^{(1)} = x_{012}^{(1)} \approx 1.71, \quad x^{(2)} = x_{012}^{(2)} \approx 1.05 \quad (29)$$

where  $\lambda^x = \lambda_{012} \approx 0.37$ . A similar approach can be used to make  $\hat{\Lambda}^y$  independent of the  $\mathbb{Z}_2$  charges, which allows the implementation of  $\hat{\mathcal{H}}_{2\text{leg}}^{\text{simp}}$  from Eq. 24.

**Realizing a  $\mathbb{Z}_2$  LGT in a 2D square lattice**

Now, we present a coupling scheme of double-wells, which results in an effective 2D LGT Hamiltonian with genuine local symmetries, in addition to the global  $U(1)$  symmetry associated with  $a$ -number conservation. We will derive a model with  $\mathbb{Z}_2$  gauge-invariant minimal coupling terms  $\sim \hat{\tau}_{(i,j)}^z \hat{a}_i^\dagger \hat{a}_j$  along all links of the square lattice.

*Setup.* We consider the setup shown in Fig. 6A in a layered 2D optical lattice, which is a particular type of brick-wall lattice. The  $a$ -particles tunnel vertically between the layers in the  $z$  direction, with coupling matrix element  $t_z^a$ , and along the links indicated in the figure with tunnel couplings  $t_x^a$  and  $t_y^a$ . Every tube consisting of four lattice sites with coordinates  $x, y$ , and  $n\mathbf{e}_z$  for  $n = 1, 2, 3, 4$  defines a supersite  $j = x\mathbf{e}_x + y\mathbf{e}_y$ , in the effective 2D lattice shown in Fig. 6B. The four links connecting every supersite to its nearest neighbors  $i : \langle i, j \rangle$  are realized by double-well systems, with exactly one  $f$ -particle each, in different layers of the optical lattice. The  $f$ -particles are only allowed to tunnel between the sites of their respective double-wells in the  $x$ - $y$  plane, with amplitudes  $t_x^f$  and  $t_y^f$ , while tunneling along the  $z$  direction is suppressed,  $t_z^f = 0$ .

For the realization of the individual double-well systems, we consider a modulated potential gradient along  $x$  and  $y$ , seen equally by

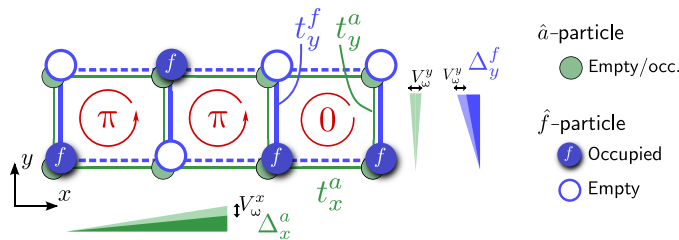


**Fig. 5. Implementing matter-gauge field coupling in a two-leg ladder.** Multiple double-well systems as described in Fig. 2 are combined to form a two-leg ladder by including hopping elements  $t_x^a$  of the  $a$ -particles along the  $x$  direction. Coherent tunneling is first suppressed by strong interspecies Hubbard interactions  $U$  and static potential gradients:  $\Delta_x^a = U$  for  $a$ -particles along  $x$ , and  $\Delta_y^f = U$  for  $f$ -particles along  $y$ . These gradients are indicated by triangles whose colors refer to the respective atomic species. The tunnel couplings are restored by a resonant lattice shaking with frequency  $\omega = U$ , realized by a modulated potential gradient  $V_\omega(\mathbf{j}, t) = (j_x V_\omega^x + j_y V_\omega^y) \cos(\omega t)$  seen by both species. The modulated gradients are indicated by light-colored triangles. We assume that each rung is occupied by exactly one  $f$ -particle, which can thus be described by a link variable, while the number  $N_a$  of  $a$ -particles is freely tunable. As shown in section S2, the special choice for the driving strengths  $V_\omega^a/\omega = V_\omega^y/\omega = x_{02}$  leads to an effective Hamiltonian with matter coupled to  $\mathbb{Z}_2$  lattice gauge fields on the rungs. The gradient  $\Delta_x^a = U$  guarantees that the  $a$ -particles pick up only trivial phases  $\hat{\phi}^x = 0$  while tunneling along the legs of the ladder. Hence, the Aharonov-Bohm phases (red) associated with the matter field become 0, or  $\pi$  corresponding to a vison excitation. They are determined by the plaquette terms  $\hat{B}_p$  defined in Eq. 20, reflecting the configuration of  $f$ -particles.

the matter and gauge fields. The modulation amplitudes  $V_\omega^x/\omega = V_\omega^y/\omega = x_{02}$  are chosen to simplify the amplitude renormalization of  $f$ -particle tunneling. As previously, we consider static potential gradients along  $x$  and  $y$  directions of  $\Delta_x^f = \Delta_y^f = U$  per site, seen only by the  $f$ -particles, and work in a regime where  $U = \omega \gg |t_\mu^v|$ , with  $\mu = x, y, z$  and  $v = a, f$ .

To realize  $a$ -particle tunneling along  $z$ , which is independent of the  $\mathbb{Z}_2$  gauge fields  $\hat{\tau}^z$  on the links in the  $x$ - $y$  plane, we add a static potential gradient of  $\Delta_z^a$  per site along the  $z$  direction. It is modulated by two frequency components  $\omega$  and  $2\omega$ , with amplitudes  $V_\omega^z$  and  $V_{2\omega}^z$ . These driving strengths are chosen as in Eq. 29, i.e.,  $V_\omega^z/\omega = x_{012}^{(1)}$  and  $V_{2\omega}^z/\omega = x_{012}^{(2)}$ , such that the restored tunnel couplings with amplitude  $t_z^a \lambda_{012}$  become independent of the  $f$ -particle configuration.

*Effective Hamiltonian.* Combining our results from the previous section, we obtain the effective hopping Hamiltonian  $\hat{\mathcal{H}}_{2\text{DLGT}}$  for the setup described in Fig. 6

$$\begin{aligned} \hat{\mathcal{H}}_{2\text{DLGT}} = & -t_{xy}^f \sum_{\langle i,j \rangle} \hat{\Lambda}_{(i,j)} \hat{v}_{(i,j)}^x \\ & - t_{xy}^a \lambda_{02} \sum_{\langle i,j \rangle} \left( \hat{\tau}_{(i,j)}^z \hat{a}_{i,m(i,j)}^\dagger \hat{a}_{j,m(i,j)} + \text{h.c.} \right) \\ & - t_z^a \lambda_{012} \sum_j \sum_{n=1}^3 \left( \hat{a}_{j,n+1}^\dagger \hat{a}_{j,n} + \text{h.c.} \right) \end{aligned} \quad (30)$$

using the same notation as introduced earlier. Here, we treat the  $z$ -coordinate  $n\mathbf{e}_z$ , with  $n = 1, \dots, 4$ , as an internal degree of freedom, while  $\mathbf{j}$  is a site index in the 2D square lattice;  $m_{(i,j)} \in \{1, 2, 3, 4\}$  denotes the  $z$ -coordinate corresponding to double well  $\langle i, j \rangle$ . For simplicity, we assumed that  $t_x^a = t_y^a = t_{xy}^a$  and  $t_x^f = t_y^f = t_{xy}^f$ . The amplitude renormalization for  $f$ -particles in the  $x$ - $y$  plane depends on the  $\mathbb{Z}_2$  charges  $\hat{Q}_{j,n}$

$$\begin{aligned} \hat{\Lambda}_{(i,j)} = & \frac{1}{2} [\mathcal{J}_0(x_{02}) + \mathcal{J}_1(x_{02})] + \hat{Q}_{i,m(i,j)} \hat{Q}_{j,m(i,j)} \frac{1}{2} \\ & [\mathcal{J}_1(x_{02}) - \mathcal{J}_0(x_{02})] \end{aligned} \quad (31)$$

Using the multifrequency driving scheme explained around Eq. 28, a situation where  $\hat{\Lambda}_{(i,j)}$  becomes independent of the  $\mathbb{Z}_2$  charges can be realized.

A simplified effective Hamiltonian, where the internal degrees of freedom are eliminated, can be obtained when  $U = \omega \gg t_z^a$  and  $\lambda_{012} t_z^a \gg t_{xy}^a$ ; the first inequality is required by the proposed implementation scheme. In this limit, the tunneling of  $a$ -particles along  $z$  can be treated independently of the in-plane tunnelings  $t_{xy}^a$ . The ground state with a single  $a$ -particle tunneling along  $z$  at supersite  $\mathbf{j}$  is  $\hat{a}_j^\dagger |0\rangle$ , where  $\hat{a}_j^\dagger = \sum_{n=1}^4 \phi_n \hat{a}_{j,n}^\dagger$ , with  $\phi_1 = \phi_4 = (5 + \sqrt{5})^{-1/2}$  and  $\phi_2 = \phi_3 = (1 + 1/\sqrt{5})^{1/2}/2$ . It is separated by an energy gap  $\Delta\epsilon = \lambda_{012} t_z^a \gg t_{xy}^a$  from the first excited state, which justifies our restriction to this lowest internal state.

The ground state energy  $\epsilon_{2a}$  with two hard-core  $a$ -particles tunneling along  $z$  in the same supersite is larger than twice the energy  $\epsilon_a$  of a single  $a$ -particle, by an amount  $U_{\text{eff}}$ , i.e.,  $\epsilon_{2a} = 2\epsilon_a + U_{\text{eff}}$ . By solving the one- and two-particle problems exactly, we find  $U_{\text{eff}} = \lambda_{012} t_z^a$ . In the effective model restricted to the lowest internal state, this offset corresponds to a repulsive Hubbard interaction on the supersites  $\mathbf{j}$ . Because  $U_{\text{eff}} \gg t_{xy}^a$ , double occupancy of supersites is strongly suppressed, and we can treat the new operators  $\hat{a}_j^{(\dagger)}$  as hard-core bosons.

By projecting the Hamiltonian (Eq. 30) to the lowest internal state on every supersite, we arrive at the following simplified model

$$\begin{aligned} \hat{\mathcal{H}}_{2\text{DLGT}}^{\text{simp}} = & \varepsilon_a \sum_j \hat{a}_j^\dagger \hat{a}_j - t_{xy}^f \sum_{\langle i,j \rangle} \hat{\Lambda}_{\langle i,j \rangle} \hat{\tau}_{\langle i,j \rangle}^x \\ & - t_{xy}^a \lambda_{02} |\phi_1|^2 \sum_{\langle i,j \rangle \in E} \left( \hat{\tau}_{\langle i,j \rangle}^z \hat{a}_i^\dagger \hat{a}_j + \text{h.c.} \right) \\ & - t_{xy}^a \lambda_{02} |\phi_2|^2 \sum_{\langle i,j \rangle \in B} \left( \hat{\tau}_{\langle i,j \rangle}^z \hat{a}_i^\dagger \hat{a}_j + \text{h.c.} \right) \end{aligned} \quad (32)$$

Here, we distinguish between two sets of links,  $\langle i,j \rangle \in E$  or  $B$ , which are realized in layers at the edge  $n = 1,4$  ( $E$ ) and in the bulk  $n = 2,3$  ( $B$ ) in the 3D implementation (see Fig. 6A). Because the internal state has different weights  $|\phi_1|^2 \approx 0.14$  and  $|\phi_2|^2 \approx 0.36$ , they are associated with different tunneling amplitudes. This complication can be avoided by realizing bare tunnelings of  $a$ -particles with different strengths on  $E$ - and  $B$ -type bonds.

**Symmetries.** In contrast to the two-leg ladder (Eq. 19), the models in Eqs. 30 and 32 are both characterized by local  $\mathbb{Z}_2$  gauge symmetries. The  $\mathbb{Z}_2$  charge on a supersite is defined as  $\hat{Q}_j = \exp[i\pi \sum_{n=1}^4 \hat{n}_{j,n}^a]$ , which becomes  $\hat{Q}_j = \exp[i\pi \hat{a}_j^\dagger \hat{a}_j]$  when projected to the lowest internal state. The  $\mathbb{Z}_2$  gauge group is generated by

$$\hat{G}_j = \hat{Q}_j \prod_{i:\langle j,i \rangle} \hat{\tau}_{\langle j,i \rangle}^x \quad (33)$$

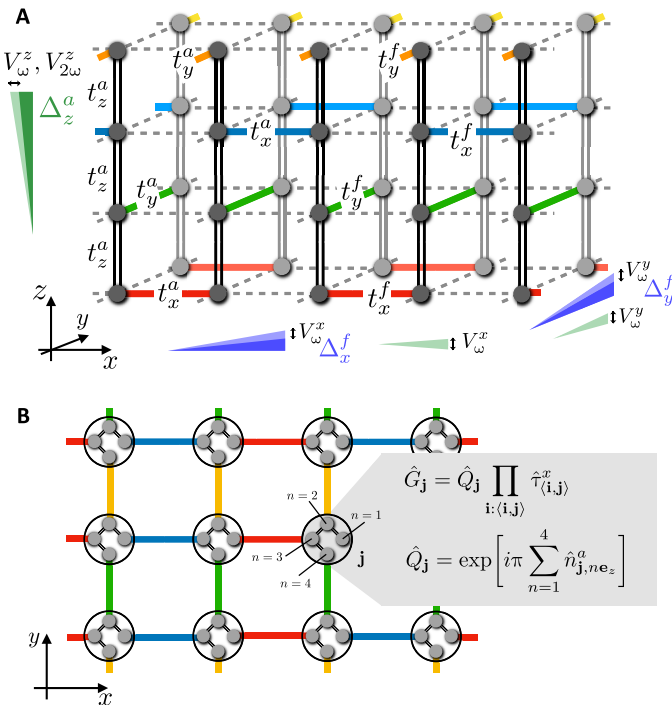


**Fig. 6. Realizing  $\mathbb{Z}_2$  LGT coupled to matter in 2D.** (A) Multiple double-well systems as described in Fig. 2 are combined in the shown brick-wall lattice. Each of its four layers along the  $z$  direction is used to realize one of the four links connecting every lattice site of the 2D square lattice (B) to its four nearest neighbors. The double-well systems are indicated by solid lines (colors), and they are only coupled by tunnelings of  $a$ -particles along the  $z$  direction, with amplitudes  $t_z^a$ . The required lattice gradients (their modulations) are indicated by (light) colored triangles. (B) The restored hopping Hamiltonian  $\hat{\mathcal{H}}_{2\text{DLGT}}$  in the 2D lattice has local symmetries  $\hat{G}_j$  associated with all lattice sites  $j$ , i.e.,  $[\hat{\mathcal{H}}_{2\text{DLGT}}, \hat{G}_j] = 0$ .

where the product on the right includes all links  $\langle j, i \rangle$  connected to site  $j$ .

It holds  $[\hat{\mathcal{H}}_{2\text{DLGT}}, \hat{G}_j] = 0$  and  $[\hat{\mathcal{H}}_{2\text{DLGT}}^{\text{simp}}, \hat{G}_j] = 0$  for all  $j$ , using the respective  $\mathbb{Z}_2$  charge operators. These results follow trivially for the first line of Eqs. 30 and 32, which contain only the operators  $\hat{\tau}_{\langle i,j \rangle}^x$  and  $\hat{n}_{j,n}^a$  ( $\hat{n}_j$ ) (see also Eq. 31). For the last two lines in the effective Hamiltonians, it is confirmed by a straightforward calculation.

In addition to the local  $\mathbb{Z}_2$  gauge invariance, the models (Eqs. 30 and 32) have a global  $U(1)$  symmetry associated with the conservation of the  $a$ -particle number. Very similar Hamiltonians have been studied in the context of strongly correlated electrons, where fractionalized phases with topological order have been identified (35). When the  $a$ -particles condense, effective models without the global  $U(1)$  symmetry can also be realized. These are in the same symmetry class as Kitaev’s toric code (28).

**DISCUSSION**

We have presented a general scheme for realizing flux attachment in 2D optical lattices, where one species of atoms becomes a source of magnetic flux for a second species. For a specific set of parameters, we demonstrated that the effective Floquet Hamiltonian describing our system has a  $\mathbb{Z}_2$  gauge structure. This allows us to implement experimentally a dynamical  $\mathbb{Z}_2$  gauge field coupled to matter using ultracold atoms, as we have shown specifically for a double-well setup, two-leg ladders, and in a 2D geometry. Because our scheme naturally goes beyond one spatial dimension, the  $\mathbb{Z}_2$  magnetic field—and the corresponding vison excitations—plays an important role in our theoretical analysis of the ground-state phase diagram. Moreover, the link variables in our system are realized by particle number imbalances on neighboring sites, making experimental implementations of our setup feasible using existing platforms [as described, e.g., in (42, 43, 45)].

Our theoretical analysis of hard-core bosons coupled to  $\mathbb{Z}_2$  link variables on the rungs of a two-leg ladder revealed an SF-to-Mott transition in the charge sector as well as a transition in the gauge sector. The latter is characterized by a spontaneously broken global  $\mathbb{Z}_2$  symmetry, but we argued that it can be considered as a precursor of the confinement-deconfinement transitions, which are ubiquitous in LGTs, high-energy physics, and strongly correlated quantum many-body system. Leveraging the powerful toolbox of quantum gas microscopy, our approach paves the way for new studies of LGTs with full resolution of the quantum mechanical wave function. This is particularly useful for analyzing string (57, 63) and topological (64) order parameters, which are at the heart of LGTs but difficult to access in more conventional settings.

As we have demonstrated, extensions of our LGT setting to 2D systems with local rather than global symmetries are possible. Here, we propose a realistic scheme to implement a genuine  $\mathbb{Z}_2$  LGT with minimal coupling of the matter to the gauge field on all links of a square lattice. On the one hand, this realizes one of the main ingredients of Kitaev’s toric code (28, 65, 66)—a specific version of an LGT coupled to matter, which displays local  $\mathbb{Z}_2$  gauge symmetry and hosts excitations with non-Abelian anyonic statistics. On the other hand, the systems that can be implemented with our technique are reminiscent of models studied in the context of nematic magnets (27, 33, 67) and strongly correlated electron systems (13, 35, 36). Other extensions of our work include studies of more general systems with flux attachment, which are expected to reveal physics related to the formation of composite fermions in the FQH effect.

Another application of our work is the realization of the recently suggested  $\mathbb{Z}_2$  Bose-Hubbard Hamiltonian (68) using ultracold atoms in optical lattices. This model contains  $\mathbb{Z}_2$  link variables on a 1D chain, similar to our case, but includes terms in the Hamiltonian, which explicitly break the local  $\mathbb{Z}_2$  gauge symmetry. In contrast to the models studied in this paper, not only the tunneling phases but also the tunneling amplitudes in the  $\mathbb{Z}_2$  Bose-Hubbard Hamiltonian depend on the  $\mathbb{Z}_2$  link variables. The  $\mathbb{Z}_2$  Bose-Hubbard model features bosonic Peierls transitions (68), which can lead to an interesting interplay of symmetry breaking and symmetry-protected topological order (52, 53).

In terms of experimental implementations, we restricted our discussion in this article to ultracold atom setups. However, other quantum simulation platforms, such as arrays of superconducting qubits (69), provide promising alternatives. Generalizations of our scheme to these systems are straightforward, and a detailed analysis of the feasibility of our proposal in such settings will be devoted to future work.

## MATERIALS AND METHODS

### Implementing dynamical gauge fields

Here, we describe in detail how synthetic gauge fields with their own quantum dynamics can be realized and implemented using ultracold atoms. We begin by quickly reviewing results for the case of a single particle in a double-well potential, which we use later on to derive the effective Hamiltonian in a many-body system.

#### Single-particle two-site problem

We consider the following Hamiltonian describing a single particle hopping between sites  $|1\rangle$  and  $|2\rangle$

$$\hat{\mathcal{H}}_2 = -t(|2\rangle\langle 1| + |1\rangle\langle 2|) + (\Delta_{2,1} + \Delta_{2,1}^{\omega}(t))|2\rangle\langle 2| \quad (34)$$

Here,  $t > 0$  denotes the bare tunnel coupling, which is strongly suppressed by the energy offset  $|\Delta_{2,1}| \gg t$ . Tunneling is then restored by a modulation

$$\Delta_{2,1}^{\omega}(t) = A_{2,1} \cos(\omega t + \phi_{2,1}) \quad (35)$$

For resonant shaking,  $\omega = \Delta_{2,1}$ , it has been shown in (47) that the dynamics of Eq. 34 can be described by the following effective Hamiltonian

$$\hat{\mathcal{H}}_{2,\text{eff}} = -\tilde{t}(|2\rangle\langle 1| e^{i\phi_{2,1}} + |1\rangle\langle 2| e^{-i\phi_{2,1}}) \quad (36)$$

The amplitude of the restored tunneling is given by

$$\tilde{t} = t \mathcal{J}_1\left(\frac{A_{2,1}}{\omega}\right) \quad (37)$$

and the complex phase  $\phi_{2,1}$  is determined directly from the modulating potential  $\Delta_{2,1}^{\omega}(t)$ .

More generally, when the offset  $\Delta_{2,1} = n\omega$  is a positive integer multiple  $n = 0, 1, 2, 3, 4, \dots$  of the driving frequency  $\omega$ , tunneling can

also be restored. As shown by a general formalism in (48), the effective Hamiltonian in this case becomes

$$\hat{\mathcal{H}}_{2,\text{eff}} = -\tilde{t}_n(|2\rangle\langle 1| e^{in\phi_{2,1}} + |1\rangle\langle 2| e^{-in\phi_{2,1}}) \quad (38)$$

For  $n = 0$ , the result is independent of the phase  $\phi_{2,1}$  of the modulation. The tunneling matrix element is renormalized by

$$\tilde{t}_n = t \mathcal{J}_n\left(\frac{A_{2,1}}{\omega}\right) \quad (39)$$

The first three Bessel functions,  $n = 0, 1, 2$ , are plotted in fig. S1 as a function of  $x = A_{2,1}/\omega$ .

Last, we consider the case when  $\Delta_{2,1} = -n\omega$ , for a positive integer  $n = 1, 2, 3, \dots$ . In this case, we can rewrite the modulation (Eq. 35) as

$$\Delta_{2,1}^{\omega}(t) = A_{2,1} \cos(-\omega t - \phi_{2,1}) \quad (40)$$

i.e., effectively  $\omega \rightarrow -\omega$  and  $\phi_{2,1} \rightarrow -\phi_{2,1}$ . By applying the results from Eqs. 38 and 39 for the system with  $-\omega$ , we obtain

$$\hat{\mathcal{H}}_{2,\text{eff}} = -\tilde{t}_n(|2\rangle\langle 1| e^{in(\pi-\phi_{2,1})} + |1\rangle\langle 2| e^{-in(\pi-\phi_{2,1})}) \quad (41)$$

The complex phase of the restored hopping in the effective Hamiltonian changes sign, because  $-\phi_{2,1}$  appears in Eq. 40. In addition, it contains a  $\pi$  phase shift, which takes into account the sign change of the renormalized tunneling matrix element  $\propto \mathcal{J}_n\left(\frac{A_{2,1}}{-\omega}\right) = e^{i\pi n} \mathcal{J}_n\left(\frac{A_{2,1}}{\omega}\right)$  if  $n$  is odd.

#### Multiple driving frequencies

Even more control over the restored tunnel couplings can be gained by using lattice modulations with multiple frequency components. Here, we summarize results for the single-particle two-site problem from above, for the case of driving with frequency components  $\omega$  and  $2\omega$ . To do so, we modify our Hamiltonian in Eq. 35 as

$$\hat{\mathcal{H}}_2 = -t(|2\rangle\langle 1| + |1\rangle\langle 2|) + \Delta_{2,1}|2\rangle\langle 2| + \Delta_{2,1}^{\omega}(t)|1\rangle\langle 1| \quad (42)$$

where the  $2\pi/\omega$ -periodic driving term takes the following form

$$\Delta_{2,1}^{\omega}(t) = A_{2,1}^{(1)} \cos(\omega t + \phi_{2,1}^{(1)}) + A_{2,1}^{(2)} \cos(2\omega t + \phi_{2,1}^{(2)}) \quad (43)$$

To calculate the effective Hamiltonian, we rewrite the time-dependent Hamiltonian (Eq. 42) in a moving frame by performing a time-dependent unitary transformation realized by the operator (48)

$$\hat{R}(t) = \exp(i\Delta_{2,1}t\hat{P}_2) \exp\left\{i\left(\frac{A_{2,1}^{(1)}}{\omega}\right) \sin(\omega t + \phi_{2,1}^{(1)})\hat{P}_1\right\} \times \exp\left\{i\left(\frac{A_{2,1}^{(2)}}{2\omega}\right) \sin(2\omega t + \phi_{2,1}^{(2)})\hat{P}_1\right\} \quad (44)$$

where we introduced the projectors  $\hat{P}_1 = |1\rangle\langle 1|$  and  $\hat{P}_2 = |2\rangle\langle 2|$ . In this moving frame, the time-dependent Hamiltonian in Eq. 42

takes the form

$$\begin{aligned} \hat{\mathcal{H}}_2 = & -t |1\rangle\langle 2| e^{-i\Delta_{2,1}t} \\ & \times e^{i\left(\frac{A_{2,1}^{(1)}}{\omega}\right) \sin(\omega t + \phi_{2,1}^{(1)})} e^{i\left(\frac{A_{2,1}^{(2)}}{2\omega}\right) \sin(\omega t + \phi_{2,1}^{(2)})} + \text{h.c.} \end{aligned} \quad (45)$$

Using the Jacobi-Anger identity

$$e^{iasin(\omega t + \phi)} = \sum_{k=-\infty}^{\infty} \mathcal{J}_k(\alpha) e^{ik(\omega t + \phi)} \quad (46)$$

and time-averaging the time-dependent Hamiltonian in Eq. 45 over a period  $T = 2\pi/\omega$  of the drive, we obtain an effective Hamiltonian of the form

$$\hat{\mathcal{H}}_{2,\text{eff}} = -|1\rangle\langle 2| \sum_{\ell=-\infty}^{\infty} \tilde{t}_{n,\ell} e^{i(n-2\ell)\phi_{2,1}^{(1)} + i\ell\phi_{2,1}^{(2)}} + \text{h.c.} \quad (47)$$

While this effective Hamiltonian is similar to Eq. 38, the amplitude renormalization now involves a product of two Bessel functions

$$\tilde{t}_{n,\ell} = t \mathcal{J}_{n-2\ell}\left(\frac{A_{2,1}^{(1)}}{\omega}\right) \mathcal{J}_{\ell}\left(\frac{A_{2,1}^{(2)}}{2\omega}\right) \quad (48)$$

### Two-particle two-site problem

Now, we apply the results from the first paragraph (Eqs. 34 to 41) to the problem of a pair of  $a$ - and  $f$ -particles in a double-well potential (see Fig. 2). In contrast to the main text, we consider general parameters in our derivation of the effective Hamiltonian. Our starting point is the model in Eqs. 1 to 6 for two sites  $\mathbf{j}_1$  and  $\mathbf{j}_2 = \mathbf{j}_1 + \mathbf{e}_y$ . We assume  $V_a(\mathbf{j}_{1,2}) \equiv 0$  but introduce a static energy offset  $\Delta^f = U$  between the two lattice sites for the  $f$ -particles,  $V_f(\mathbf{j}_2) = \Delta^f + V_f(\mathbf{j}_1)$ . Because our analysis is restricted to the subspace with one  $a$ -particle and one  $f$ -particle, the hard-core constraint assumed in the main text is not required in this case and the statistics of the two species are irrelevant.

The two-site problem has four basis states,  $\hat{f}_{j_m}^\dagger \hat{a}_{j_n}^\dagger |0\rangle$  with  $m, n = 1, 2$ . Their corresponding on-site energies are 0,  $\Delta^f = U$ ,  $U$ ,  $\Delta^f + U = 2U$  (see fig. S2A), which suppress most coherent tunneling processes because  $\Delta^f = U \gg |t_y^a|, |t_y^f|$ . When the resonant lattice modulation  $\hat{\mathcal{H}}_\omega(t)$  with frequency  $\omega = U$  is included, all tunnel couplings are restored. Now, we will show that the effective Floquet Hamiltonian is given by

$$\hat{\mathcal{H}}_{\text{eff}}^{2\text{well}} = -t_y^a \lambda e^{i\hat{\phi}} \hat{a}_{j_2}^\dagger \hat{a}_{j_1} - t_y^f \hat{\Lambda} e^{i\hat{\theta}} \hat{\tau}_{(j_2, j_1)}^+ + \text{h.c.} \quad (49)$$

where  $\hat{\tau}_{(j_2, j_1)}^+ = \hat{f}_{j_2}^\dagger \hat{f}_{j_1}$  and

$$\hat{\phi} = \phi_{j_2, j_1} + (1 - \hat{\tau}_{(j_2, j_1)}^z) \left( \frac{\pi}{2} - \phi_{j_2, j_1} \right) \quad (50)$$

$$\lambda = \mathcal{J}_1(A_{j_2, j_1}/\omega) \quad (51)$$

$$\hat{\theta} = 2\phi_{j_2, j_1} \hat{n}_{j_2}^a \quad (52)$$

$$\hat{\Lambda} = \mathcal{J}_0(A_{j_2, j_1}/\omega) \hat{n}_{j_1}^a + \mathcal{J}_2(A_{j_2, j_1}/\omega) \hat{n}_{j_2}^a \quad (53)$$

To derive Eqs. 49 to 53, we first consider the effect of the coherent driving  $\hat{\mathcal{H}}_\omega(t)$ , characterized by Eq. 9, on the matter field  $\hat{a}$ . Because the Hamiltonian

$$\begin{aligned} \hat{\mathcal{H}}^a = & -t_y^a \left( \hat{a}_{j_2}^\dagger \hat{a}_{j_1} + \text{h.c.} \right) + (\hat{n}_{j_2}^a - \hat{n}_{j_1}^a) \\ & \times \frac{1}{2} \left( U \hat{\tau}_{(j_2, j_1)}^z + V_\omega(j_2, t) - V_\omega(j_1, t) \right) \end{aligned} \quad (54)$$

governing the dynamics of  $\hat{a}$ , commutes with the link variable, characterizing the gauge field,  $[\hat{\mathcal{H}}^a, \hat{\tau}_{(j_2, j_1)}^z] = 0$ , we can treat  $\hat{\tau}_{(j_2, j_1)}^z$  as a  $\mathbb{C}$ -number with two possible values,  $\pm 1$ .

When expressed in terms of the two states  $|1\rangle_a = \hat{a}_{j_1}^\dagger |0\rangle$  and  $|2\rangle_a = \hat{a}_{j_2}^\dagger |0\rangle$ , the Hamiltonian  $\hat{\mathcal{H}}^a$  is of the same form as  $\hat{\mathcal{H}}_2$  in Eq. 34. It has an energy difference of  $\Delta_{2,1} = U \hat{\tau}_{(j_2, j_1)}^z$  between the two states, which is caused microscopically by the interspecies Hubbard interaction  $U$  (see fig. S2A).

According to Eqs. 38 and 41, the restored tunnel coupling between  $|1\rangle_a$  and  $|2\rangle_a$  has a complex phase given by  $\varphi = \phi_{j_2, j_1}$  if  $\Delta_{2,1} > 0$ , i.e., for  $\hat{\tau}_{(j_2, j_1)}^z = 1$ , and it is  $\varphi = \pi - \phi_{j_2, j_1}$  if  $\Delta_{2,1} < 0$ , i.e., for  $\hat{\tau}_{(j_2, j_1)}^z = -1$ . Because in both cases the magnitude of the energy mismatch between the two sites is  $|\Delta_{2,1}| = \omega$ , the tunneling is renormalized by  $\lambda = \mathcal{J}_1(A_{j_2, j_1}/\omega)$ . These results confirm Eqs. 50 and 51.

Next, we consider the dynamics of the  $f$ -particles or, equivalently, the link variable  $\hat{\tau}_{(j_2, j_1)}^z$ . It is governed by the following Hamiltonian

$$\begin{aligned} \hat{\mathcal{H}}^f = & -t_y^f \left( \hat{\tau}_{(j_2, j_1)}^+ + \text{h.c.} \right) + \hat{\tau}_{(j_2, j_1)}^z \\ & \times \frac{1}{2} \left( \Delta^f + U \delta \hat{n}^a + V_\omega(j_2, t) - V_\omega(j_1, t) \right) \end{aligned} \quad (55)$$

Because  $\hat{\mathcal{H}}^f$  commutes with the matter field,  $[\hat{\mathcal{H}}^f, \hat{n}_{j_1}^a] = [\hat{\mathcal{H}}^f, \hat{n}_{j_2}^a] = 0$ , we can treat the particle number imbalance

$$\delta \hat{n}^a = \hat{n}_{j_2}^a - \hat{n}_{j_1}^a \quad (56)$$

as a  $\mathbb{C}$ -number now, which can take two values  $\pm 1$ .

When expressed in terms of the two states  $|1\rangle_f = \hat{f}_{j_1}^\dagger |0\rangle$  and  $|2\rangle_f = \hat{f}_{j_2}^\dagger |0\rangle$ , the Hamiltonian  $\hat{\mathcal{H}}^f$  is of the same form as  $\hat{\mathcal{H}}_2$  in Eq. 34. It has an energy difference of  $\Delta_{2,1} = \Delta^f + U \delta \hat{n}^a$  between the two states, which is caused microscopically by the interspecies Hubbard interaction  $U$  and the potential gradient  $\Delta^f$ , which the  $f$ -particles are subject to (see fig. S2A).

In the case of  $f$ -particles, the energy offset  $\Delta_{2,1}$  can only take positive values 0 and  $2\omega$  if  $\Delta^f = U = \omega$ . From Eq. 38, it follows that the restored tunnel coupling between  $|1\rangle_f$  and  $|2\rangle_f$  has a complex phase given by  $\theta = 0$  if  $\Delta_{2,1} = 0$ , i.e., for  $\delta \hat{n}^a = -1$ , and by  $\theta = 2\phi_{j_2, j_1}$  if  $\Delta_{2,1} = 2\omega$ , i.e., for  $\delta \hat{n}^a = 1$ . Expressed in terms of  $\hat{n}_{j_2}^a$ , in a subspace where  $\hat{n}_{j_1}^a + \hat{n}_{j_2}^a = 1$ , this result confirms Eq. 52.

The magnitudes of the restored tunneling couplings of  $f$ -particles in the two-particle Hilbert space depend on the energy offset  $\Delta_{2,1}$ . In the case when  $\Delta_{2,1} = 0$ , i.e., for  $\delta \hat{n}^a = -1$ , it becomes  $\Lambda t_y^f = t_y^f \mathcal{J}_0(A_{j_2, j_1}/\omega)$ . When  $\Delta_{2,1} = 2\omega$ , i.e., for  $\delta \hat{n}^a = 1$ , it is given another Bessel function,  $\Lambda t_y^f = t_y^f \mathcal{J}_2(A_{j_2, j_1}/\omega)$ . This result, summarized in fig. S2B, confirms Eq. 53.

### Realizations with ultracold atoms

Next, we discuss realizations of the two-particle two-site problem with ultracold atoms. The proposed implementation needs two distinguishable particles with strong interspecies on-site interaction

energy  $U \gg t_s$ . The particles occupy a double well with both species-dependent and species-independent on-site potentials. For the species-dependent contribution, a static potential is sufficient, which introduces a tilt  $\Delta^f = U$  between neighboring sites for the  $f$ -particles but leads to zero tilt for the  $a$ -particles. On the other hand, the species-independent contribution must be time-dependent  $V_\omega(t)$  to restore resonant tunneling for both particles.

For ultracold atoms, a cubic array of lattice sites with period  $d_s$  can be created by three mutually orthogonal standing waves with wavelengths  $\lambda = 2d_s$ . When extending this simple cubic lattice along one axis by an additional lattice with twice the period  $d_l = 2d_s$ , a superlattice of the form  $V_s \sin^2(\pi y/d_s + \pi/2) + V_l \sin^2(\pi y/d_l + \phi_{SL}/2)$  arises. In the limit  $V_l \gg V_s$ , the superlattice potential resembles a chain of double wells, where tunneling between each double well is suppressed and all dynamics is restricted to two sites. Tuning the relative phase  $\phi_{SL}$  allows dynamic control of the on-site potentials. In principle, the time-dependent modulation  $V_\omega(t)$  can be implemented by a fast modulation of  $\phi_{SL}$ ; however, the modulation frequency may be limited to small values depending on the implementation of the lattices. For a superlattice with a common retroreflector, for instance, the phase  $\phi_{SL}$  can only be varied by changing the frequency of the laser. Alternatively, a second lattice  $V_{mod} \sin^2(\pi y/d_l + \phi_{mod}/2)$  with period  $d_l$  and phase  $\phi_{mod} = \pm\pi/2$  can be introduced such that it only affects the on-site potential of a single site of the double well. Therefore, amplitude modulation  $V_{mod}(t)$  of this additional lattice induces a relative modulation of the on-site energies. This leads to a nonzero species-independent, time averaged energy offset, which can be compensated by the static phase degree of freedom  $\phi_{SL}$  of the superlattice.

The two distinguishable particles can be encoded in different hyperfine sublevels with different magnetic moments, enabling the direct implementation of the static species-dependent potentials by a magnetic field gradient. This is especially appealing for bosonic atoms having a hyperfine sublevel with zero magnetic moment, which directly results in a vanishing, magnetic field-independent tilt for the  $a$ -particles in first order. Nevertheless, this is not essential as tilts for the  $a$ -particles can be compensated by the present species-independent potentials.

## SUPPLEMENTARY MATERIALS

Supplementary material for this article is available at <http://advances.sciencemag.org/cgi/content/full/5/10/eaav7444/DC1>

Section S1. Flux attachment in 2D

Section S2. Implementing matter coupled to a  $\mathbb{Z}_2$  gauge field in the two-leg ladder geometry

Section S3. Gauge structure of two-leg ladders

Section S4. Phase transitions of gauge and matter fields

Fig. S1. Renormalized tunneling amplitudes determined by Bessel functions.

Fig. S2. Two-site two-particle problem.

Fig. S3. Flux attachment in a 2D Hofstadter model.

Fig. S4. Derivation of the effective Hamiltonian.

Fig. S5. Wilson loop scaling.

Fig. S6. The Green's function in the charge sector.

Fig. S7. The Luttinger-K parameter.

Fig. S8. Rung-Mott state at commensurate filling.

Fig. S9. Phase diagram of the  $\mathbb{Z}_2$  LGT on a two-leg ladder for commensurate filling.

Fig. S10. Transition in the gauge sector.

References (70–74)

## REFERENCES AND NOTES

- Z. F. Ezawa, *Quantum Hall Effects: Field Theoretical Approach and Related Topics Second Edition* (World Scientific Publishing Company, 2008).
- J. Dalibard, F. Gerbier, G. Juzeliūnas, P. Öhberg, Colloquium: Artificial gauge potentials for neutral atoms. *Rev. Mod. Phys.* **83**, 1523–1543 (2011).
- N. Goldman, G. Juzeliūnas, P. Öhberg, I. B. Spielman, Light-induced gauge fields for ultracold atoms. *Rep. Prog. Phys.* **77**, 126401 (2014).
- N. R. Cooper, Rapidly rotating atomic gases. *Adv. Phys.* **57**, 539–616 (2008).
- N. Gemelke, E. Sarajlic, S. Chu, Rotating few-body atomic systems in the fractional quantum Hall regime. arXiv:1007.2677 [cond-mat.quant-gas] (15 July 2010).
- V. Galitski, I. B. Spielman, Spin-orbit coupling in quantum gases. *Nature* **494**, 49–54 (2013).
- M. Aidelsburger, M. Atala, S. Nascimbène, S. Trotzky, Y.-A. Chen, I. Bloch, Experimental realization of strong effective magnetic fields in an optical lattice. *Phys. Rev. Lett.* **107**, 255301 (2011).
- J. Struck, M. Weinberg, C. Ölschläger, P. Windpassinger, J. Simonet, K. Sengstock, R. Höppner, P. Hauke, A. Eckardt, M. Lewenstein, L. Mathey, Engineering ising-XY spin-models in a triangular lattice using tunable artificial gauge fields. *Nat. Phys.* **9**, 738–743 (2013).
- G. Jotzu, M. Messer, R. Desbuquois, M. Lebrat, T. Uehlinger, D. Greif, T. Esslinger, Experimental realization of the topological Haldane model with ultracold fermions. *Nature* **515**, 237–240 (2014).
- N. Goldman, J. C. Budich, P. Zoller, Topological quantum matter with ultracold gases in optical lattices. *Nat. Phys.* **12**, 639–645 (2016).
- N. R. Cooper, J. Dalibard, I. B. Spielman, Topological bands for ultracold atoms. *Rev. Mod. Phys.* **91**, 015005 (2019).
- J. B. Kogut, An introduction to lattice gauge theory and spin systems. *Rev. Mod. Phys.* **51**, 659–713 (1979).
- T. Senthil, M. P. A. Fisher,  $\mathbb{Z}_2$  gauge theory of electron fractionalization in strongly correlated systems. *Phys. Rev. B* **62**, 7850–7881 (2000).
- T. Keilmann, S. Lanzmich, I. McCulloch, M. Roncaglia, Statistically induced phase transitions and anyons in 1d optical lattices. *Nat. Commun.* **2**, 361 (2011).
- S. Greschner, G. Sun, D. Poletti, L. Santos, Density-dependent synthetic gauge fields using periodically modulated interactions. *Phys. Rev. Lett.* **113**, 215303 (2014).
- S. Greschner, L. Santos, Anyon Hubbard model in one-dimensional optical lattices. *Phys. Rev. Lett.* **115**, 053002 (2015).
- A. Bermudez, D. Porras, Interaction-dependent photon-assisted tunneling in optical lattices: A quantum simulator of strongly-correlated electrons and dynamical gauge fields. *New J. Phys.* **17**, 103021 (2015).
- C. Sträter, S. C. L. Srivastava, A. Eckardt, Floquet realization and signatures of one-dimensional anyons in an optical lattice. *Phys. Rev. Lett.* **117**, 205303 (2016).
- L. W. Clark, B. M. Anderson, L. Feng, A. Gaj, K. Levin, C. Chin, Observation of density-dependent gauge fields in a Bose-Einstein condensate based on micromotion control in a shaken two-dimensional lattice. *Phys. Rev. Lett.* **121**, 030402 (2018).
- U.-J. Wiese, Ultracold quantum gases and lattice systems: Quantum simulation of lattice gauge theories. *Ann. Phys.* **525**, 777–796 (2013).
- E. Zohar, J. I. Cirac, B. Reznik, Quantum simulations of lattice gauge theories using ultracold atoms in optical lattices. *Rep. Prog. Phys.* **79**, 014401 (2016).
- M. Dalmonte, S. Montangero, Lattice gauge theory simulations in the quantum information era. *Contemp. Phys.* **57**, 388–412 (2016).
- E. A. Martinez, C. A. Muschik, P. Schindler, D. Nigg, A. Erhard, M. Heyl, P. Hauke, M. Dalmonte, T. Monz, P. Zoller, R. Blatt, Real-time dynamics of lattice gauge theories with a few-qubit quantum computer. *Nature* **534**, 516–519 (2016).
- E. Zohar, A. Farace, B. Reznik, J. I. Cirac, Digital quantum simulation of  $\mathbb{Z}_2$  lattice gauge theories with dynamical fermionic matter. *Phys. Rev. Lett.* **118**, 070501 (2017).
- T. V. Zache, F. Hebenstreit, F. Jendrzejewski, M. K. Oberthaler, J. Berges, P. Hauke, Quantum simulation of lattice gauge theories using Wilson fermions. *Quantum Sci. Technol.* **3**, 034010 (2018).
- E. Fradkin, S. H. Shenker, Phase diagrams of lattice gauge theories with Higgs fields. *Phys. Rev. D* **19**, 3682–3697 (1979).
- P. E. Lammert, D. S. Rokhsar, J. Toner, Topology and nematic ordering. I. A gauge theory. *Phys. Rev. E* **52**, 1778–1800 (1995).
- A. Y. Kitaev, Fault-tolerant quantum computation by anyons. *Ann. Phys.* **303**, 2–30 (2003).
- F. Wilczek, Magnetic flux, angular momentum, and statistics. *Phys. Rev. Lett.* **48**, 1144–1146 (1982).
- F. Wilczek, Quantum mechanics of fractional-spin particles. *Phys. Rev. Lett.* **49**, 957–959 (1982).
- P. A. Lee, From high temperature superconductivity to quantum spin liquid: Progress in strong correlation physics. *Rep. Prog. Phys.* **71**, 012501 (2008).
- S. Sachdev, N. Read, Large N expansion for frustrated and doped quantum antiferromagnets. *Int. J. Mod. Phys. B* **5**, 219 (1991).
- D. Podolsky, E. Demler, Properties and detection of spin nematic order in strongly correlated electron systems. *New J. Phys.* **7**, 59 (2005).
- S. Gazit, M. Randeria, A. Vishwanath, Emergent Dirac fermions and broken symmetries in confined and deconfined phases of  $\mathbb{Z}_2$  gauge theories. *Nat. Phys.* **13**, 484–490 (2017).

35. R. D. Sedgewick, D. J. Scalapino, R. L. Sugar, Fractionalized phase in an XY-Z<sub>2</sub> gauge model. *Phys. Rev. B* **65**, 054508 (2002).
36. E. Demler, C. Nayak, H.-Y. Kee, Y. B. Kim, T. Senthil, Fractionalization patterns in strongly correlated electron systems: Spin-charge separation and beyond. *Phys. Rev. B* **65**, 155103 (2002).
37. R. K. Kaul, Y. B. Kim, S. Sachdev, T. Senthil, Algebraic charge liquids. *Nat. Phys.* **4**, 28 (2007).
38. S. Sachdev, D. Chowdhury, The novel metallic states of the cuprates: Topological Fermi liquids and strange metals. *Prog. Theor. Exp. Phys.* **2016**, 12C102 (2016).
39. C. Schweizer, F. Grusdt, M. Berggruber, L. Barbiero, E. Demler, N. Goldman, I. Bloch, M. Aidelsburger, Floquet approach to Z<sub>2</sub> lattice gauge theories with ultracold atoms in optical lattices. *Nat. Phys.* 10.1038/s41567-019-0649-7 (2019).
40. F. Görg, K. Sandholzer, J. Minguzzi, R. Desbuquois, M. Messer, T. Esslinger, Realization of density-dependent Peierls phases to engineer quantized gauge fields coupled to ultracold matter. *Nat. Phys.* 10.1038/s41567-019-0615-4 (2019).
41. M. Aidelsburger, M. Atala, M. Lohse, J. T. Barreiro, B. Paredes, I. Bloch, Realization of the Hofstadter Hamiltonian with ultracold atoms in optical lattices. *Phys. Rev. Lett.* **111**, 185301 (2013).
42. H. Miyake, G. A. Siviloglou, C. J. Kennedy, W. C. Burton, W. Ketterle, Realizing the Harper Hamiltonian with laser-assisted tunneling in optical lattices. *Phys. Rev. Lett.* **111**, 185302 (2013).
43. M. Aidelsburger, M. Lohse, C. Schweizer, M. Atala, J. T. Barreiro, S. Nascimbene, N. R. Cooper, I. Bloch, N. Goldman, Measuring the Chern number of Hofstadter bands with ultracold bosonic atoms. *Nat. Phys.* **11**, 162–166 (2015).
44. C. J. Kennedy, W. C. Burton, W. C. Chung, W. Ketterle, Observation of Bose-Einstein condensation in a strong synthetic magnetic field. *Nat. Phys.* **11**, 859–864 (2015).
45. M. E. Tai, A. Lukin, M. Rispoli, R. Schittko, T. Menke, D. Borgnia, P. M. Preiss, F. Grusdt, A. M. Kaufman, M. Greiner, Microscopy of the interacting Harper-Hofstadter model in the two-body limit. *Nature* **546**, 519–523 (2017).
46. D. Jaksch, P. Zoller, Creation of effective magnetic fields in optical lattices: The Hofstadter butterfly for cold neutral atoms. *New J. Phys.* **5**, 56 (2003).
47. A. R. Kolovsky, Creating artificial magnetic fields for cold atoms by photon-assisted tunneling. *Europhys. Lett.* **93**, 20003 (2011).
48. N. Goldman, J. Dalibard, M. Aidelsburger, N. R. Cooper, Periodically driven quantum matter: The case of resonant modulations. *Phys. Rev. A* **91**, 033632 (2015).
49. Y.-A. Chen, S. Nascimbene, M. Aidelsburger, M. Atala, S. Trotzky, I. Bloch, Controlling correlated tunneling and superexchange interactions with ac-driven optical lattices. *Phys. Rev. Lett.* **107**, 210405 (2011).
50. R. E. Prange, S. M. Girvin, *The Quantum Hall Effect* (Springer-Verlag, 1990).
51. J. K. Jain, Theory of the fractional quantum hall-effect. *Phys. Rev. B* **41**, 7653–7665 (1990).
52. D. González-Cuadra, A. Dauphin, P. R. Grzybowski, P. Wójcik, M. Lewenstein, A. Bermudez, Symmetry-breaking topological insulators in the Z<sub>2</sub> Bose-Hubbard model. *Phys. Rev. B* **99**, 045139 (2019).
53. D. González-Cuadra, A. Bermudez, P. R. Grzybowski, M. Lewenstein, A. Dauphin, Interwined topological phases induced by emergent symmetry protection. *Nat. Commun.* **10**, 2694 (2019).
54. S. R. White, Density matrix formulation for quantum renormalization groups. *Phys. Rev. Lett.* **69**, 2863–2866 (1992).
55. F. Crépín, N. Laflorencie, G. Roux, P. Simon, Phase diagram of hard-core bosons on clean and disordered two-leg ladders: Mott insulator–Luttinger liquid–Bose glass. *Phys. Rev. B* **84**, 054517 (2011).
56. E. Berg, E. G. Dalla Torre, T. Giamarchi, E. Altman, Rise and fall of hidden string order of lattice bosons. *Phys. Rev. B* **77**, 245119 (2008).
57. M. Endres, M. Cheneau, T. Fukuhara, C. Weitenberg, P. Schauß, C. Gross, L. Mazza, M. C. Banuls, L. Pollet, I. Bloch, S. Kuhr, Observation of correlated particle-hole pairs and string order in low-dimensional Mott insulators. *Science* **334**, 200–203 (2011).
58. S. Fazzini, F. Becca, A. Montorsi, Nonlocal parity order in the two-dimensional Mott insulator. *Phys. Rev. Lett.* **118**, 157602 (2017).
59. M. A. Cazalilla, R. Citro, T. Giamarchi, E. Orignac, M. Rigol, One dimensional bosons: From condensed matter systems to ultracold gases. *Rev. Mod. Phys.* **83**, 1405–1466 (2011).
60. M. Piraud, F. Heidrich-Meisner, I. P. McCulloch, S. Greschner, T. Vekua, U. Schollwöck, Vortex and Meissner phases of strongly interacting bosons on a two-leg ladder. *Phys. Rev. B* **91**, 140406 (2015).
61. M. Knap, A. Kantian, T. Giamarchi, I. Bloch, M. D. Lukin, E. Demler, Probing real-space and time-resolved correlation functions with many-body Ramsey interferometry. *Phys. Rev. Lett.* **111**, 147205 (2013).
62. T. Giamarchi, *Quantum Physics in One Dimension* (Oxford Univ. Press, 2003).
63. T. A. Hilker, G. Salomon, F. Grusdt, A. Omran, M. Boll, E. Demler, I. Bloch, C. Gross, Revealing hidden antiferromagnetic correlations in doped Hubbard chains via string correlators. *Science* **357**, 484–487 (2017).
64. F. Grusdt, N. Y. Yao, D. Abanin, M. Fleischhauer, E. Demler, Interferometric measurements of many-body topological invariants using mobile impurities. *Nat. Commun.* **7**, 11994 (2016).
65. B. Paredes, I. Bloch, Minimum instances of topological matter in an optical plaquette. *Phys. Rev. A* **77**, 023603 (2008).
66. H.-N. Dai, B. Yang, A. Reingruber, H. Sun, X.-F. Xu, Y.-A. Chen, Z.-S. Yuan, J.-W. Pan, Four-body ring-exchange interactions and anyonic statistics within a minimal toric-code Hamiltonian. *Nat. Phys.* **13**, 1195–1200 (2017).
67. P. E. Lammert, D. S. Rokhsar, J. Toner, Topology and nematic ordering. *Phys. Rev. Lett.* **70**, 1650–1653 (1993).
68. D. González-Cuadra, P. R. Grzybowski, A. Dauphin, M. Lewenstein, Strongly correlated bosons on a dynamical lattice. *Phys. Rev. Lett.* **121**, 090402 (2018).
69. A. A. Houck, H. E. Türeci, J. Koch, On-chip quantum simulation with superconducting circuits. *Nat. Phys.* **8**, 292–299 (2012).
70. M. Di Dio, S. De Palo, E. Orignac, R. Citro, M.-L. Chiofalo, Persisting Meissner state and incommensurate phases of hard-core boson ladders in a flux. *Phys. Rev. B* **92**, 060506 (2015).
71. C. Romen, A. M. Läuchli, Chiral Mott insulators in frustrated Bose-Hubbard models on ladders and two-dimensional lattices: A combined perturbative and density matrix renormalization group study. *Phys. Rev. B* **98**, 054519 (2018).
72. Sutherland, *Beautiful Models, 70 Years of Exactly Solved Quantum Many-Body Problems* (World Scientific, 2004).
73. M. Ogata, H. Shiba, Bethe-ansatz wave function, momentum distribution, and spin correlation in the one-dimensional strongly correlated Hubbard model. *Phys. Rev. B* **41**, 2326–2338 (1990).
74. H. V. Kruijs, I. P. McCulloch, Z. Nussinov, J. Zaanen, Geometry and the hidden order of Luttinger liquids: The universality of squeezed space. *Phys. Rev. B* **70**, 075109 (2004).

**Acknowledgments:** We thank I. Bloch and M. Lohse for fruitful discussions. We also acknowledge discussions with P. Hauke, P. Zoller, V. Kasper, A. Bermudez, L. Santos, I. Carusotto, and M. Hafezi. **Funding:** The work in Brussels was supported by the FRS-FNRS (Belgium) and the ERC Starting Grant TopoCold. The research in Munich was supported by the Deutsche Forschungsgemeinschaft (DFG, German Research Foundation) via Research Unit FOR 2414 under project number 277974659 and under Germany's Excellence Strategy - EXC2111 - 390814868, the European Commission (UQUAM grant no. 5319278), and the Nanosystems Initiative Munich (NIM) grant no. EXC4. The work at Harvard was supported by the Gordon and Betty Moore Foundation through the EPiQS program, Harvard-MIT CUA, NSF grant no. DMR-1308435, AFOSR MURI Quantum Phases of Matter (grant FA9550-14-1-0035), and AFOSR MURI: Photonic Quantum Matter (award FA95501610323). F.G. also acknowledges support from the Technical University of Munich—Institute for Advanced Study, funded by the German Excellence Initiative and the European Union FP7 under grant agreement 291763, from the DFG grant no. KN 1254/1-1, and DFG TRR80 (Project F8). **Author contributions:** F.G. and N.G. devised the initial concepts. F.G. performed the main analytical calculations, with inputs from N.G. and E.D. All DMRG simulations were performed by L.B. The proposed experimental implementation was devised by C.S., M.A., N.G., and F.G. All authors contributed substantially to the analysis of the theoretical results. The manuscript was prepared by F.G., N.G., L.B., and C.S., with inputs from all other authors. **Competing interests:** The authors declare that they have no competing interests. **Data materials and availability:** All data needed to evaluate the conclusions in the paper are present in the paper and/or the Supplementary Materials. Additional data related to this paper may be requested from the authors.

Submitted 16 October 2018

Accepted 18 September 2019

Published 11 October 2019

10.1126/sciadv.aav7444

**Citation:** L. Barbiero, C. Schweizer, M. Aidelsburger, E. Demler, N. Goldman, F. Grusdt, Coupling ultracold matter to dynamical gauge fields in optical lattices: From flux attachment to Z<sub>2</sub> lattice gauge theories. *Sci. Adv.* **5**, eaav7444 (2019).

## Coupling ultracold matter to dynamical gauge fields in optical lattices: From flux attachment to $\mathbb{Z}_2$ lattice gauge theories

Luca BarbieroChristian SchweizerMonika AidelsburgerEugene DemlerNathan GoldmanFabian Grusdt

*Sci. Adv.*, 5 (10), eaav7444. • DOI: 10.1126/sciadv.aav7444

### View the article online

<https://www.science.org/doi/10.1126/sciadv.aav7444>

### Permissions

<https://www.science.org/help/reprints-and-permissions>

Use of this article is subject to the [Terms of service](#)

---

*Science Advances* (ISSN 2375-2548) is published by the American Association for the Advancement of Science, 1200 New York Avenue NW, Washington, DC 20005. The title *Science Advances* is a registered trademark of AAAS.

Copyright © 2019 The Authors, some rights reserved; exclusive licensee American Association for the Advancement of Science. No claim to original U.S. Government Works. Distributed under a Creative Commons Attribution NonCommercial License 4.0 (CC BY-NC).